B/Ca in planktonic foraminifera as a proxy for surface seawater pH

Jimin Yu,[1] Henry Elderfield,[1] and Bärbel Hönisch[2,3]

Received 15 July 2006; revised 25 October 2006; accepted 8 November 2006; published 12 April 2007.

[1] Boron isotope systematics indicate that boron incorporation into foraminiferal $CaCO_3$ is determined by the partition coefficient, K_D ($= \frac{[B/Ca]_{CaCO_3}}{[B(OH)_4^-/HCO_3^-]_{seawater}}$), and $[B(OH)_4^-/HCO_3^-]_{seawater}$, providing, in principle, a method to estimate seawater pH and PCO_2. We have measured B/Ca ratios in *Globigerina bulloides* and *Globorotalia inflata* for a series of core tops from the North Atlantic and the Southern Ocean and in *Globigerinoides ruber* (white) from Ocean Drilling Program (ODP) site 668B on the Sierra Leone Rise in the eastern equatorial Atlantic. B/Ca ratios in these species of planktonic foraminifera seem unaffected by dissolution on the seafloor. K_D shows a strong species-specific dependence on calcification temperature, which can be corrected for using the Mg/Ca temperature proxy. A preliminary study of *G. inflata* from Southern Ocean sediment core CHAT 16K suggests that temperature-corrected B/Ca was ~30% higher during the last glacial. Correspondingly, pH was 0.15 units higher and aqueous PCO_2 was 95 μatm lower at this site at the Last Glacial Maximum. The covariation between reconstructed PCO_2 and the atmospheric pCO_2 from the Vostok ice core demonstrates the feasibility of using B/Ca in planktonic foraminifera for reconstructing past variations in pH and PCO_2.

Citation: Yu, J., H. Elderfield, and B. Hönisch (2007), B/Ca in planktonic foraminifera as a proxy for surface seawater pH, *Paleoceanography*, *22*, PA2202, doi:10.1029/2006PA001347.

1. Introduction

[2] Boron isotopic compositions of marine carbonates have been used to estimate paleo-CO_2 concentrations for periods older than available from ice cores [*Spivack et al.*, 1993; *Palmer et al.*, 1998; *Pearson and Palmer*, 1999; *Pearson and Palmer*, 2000] and to reconstruct surface pH variations on glacial/interglacial timescales [*Sanyal et al.*, 1997; *Sanyal and Bijma*, 1999; *Palmer and Pearson*, 2003; *Hönisch and Hemming*, 2005]. The principle of the $\delta^{11}B$ method is based on the speciation of boron in seawater. Dissolved boron in seawater exists primarily as a mixture of the mononuclear species $B(OH)_3$ (boric acid) and $B(OH)_4^-$ (borate), the proportions of which are highly pH-dependent (Figure 1a). Boron isotopes are fractionated between the two species (Figure 1b) and because the boron isotopic composition of marine carbonates falls close to the isotopic composition of borate, $B(OH)_4^-$ is thought to be the species incorporated into carbonates [*Hemming and Hanson*, 1992]:

$$CaCO_3 + B(OH)_4^- \rightarrow Ca(HBO_3) + HCO_3^- + H_2O \quad (1)$$

[3] The selective incorporation of $B(OH)_4^-$ into $CaCO_3$ also has implications for boron concentrations in $CaCO_3$. It follows from equation (1) that the partition coefficient, K_D, between calcium carbonate and seawater is defined as:

$$K_D = \frac{[HBO_3^{2-}/CO_3^{2-}]_{CaCO_3}}{[B(OH)_4^-/HCO_3^-]_{seawater}} = \frac{[B/Ca]_{CaCO_3}}{[B(OH)_4^-/HCO_3^-]_{seawater}} \quad (2)$$

or

$$[B/Ca]_{CaCO_3} = K_D \cdot [B(OH)_4^-/HCO_3^-]_{seawater} \quad (3)$$

[4] In the modern ocean, the $[B(OH)_4^-/HCO_3^-]_{seawater}$ ratio is proportional to pH as the concentration of $B(OH)_4^-$ increases, and that of HCO_3^- decreases, with increasing seawater pH. The oceanic residence time of boron has been estimated to be 14–20 m.y. [*Spivack and Edmond*, 1987; *Lemarchand et al.*, 2000; *Lemarchand et al.*, 2002], and thus substantial fluctuations of boron concentration, $[B]_{tot}$, are unlikely over periods shorter than a few millions of years. Coupling between seawater $[B(OH)_4^-/HCO_3^-]$ and pH would be expected for at least the Pleistocene glacial/interglacial cycles. For surface waters in equilibrium with the atmosphere, $[B(OH)_4^-/HCO_3^-]_{seawater}$ ratios should be elevated in glacial times when atmospheric pCO_2 was lower and surface water pH and salinity were higher. Therefore if the K_D in equation (3) is constant, or can be quantified, it should be possible in principle to estimate paleo-pH values of seawater using boron concentrations in marine calcium carbonate.

[5] Positive correlations between B abundance and $\delta^{11}B$ have been observed in marine carbonates (high-Mg calcite, calcite, and aragonite) [*Hemming and Hanson*, 1992], in inorganic calcite precipitated in the laboratory [*Sanyal et al.*,

[1]Godwin Laboratory for Palaeoclimate Research, Department of Earth Sciences, University of Cambridge, Cambridge, UK.
[2]MARUM, University of Bremen, Bremen, Germany.
[3]Now at Lamont-Doherty Earth Observatory of Columbia University, Palisades, New York, USA.

0883-8305/07/2006PA001347$12.00

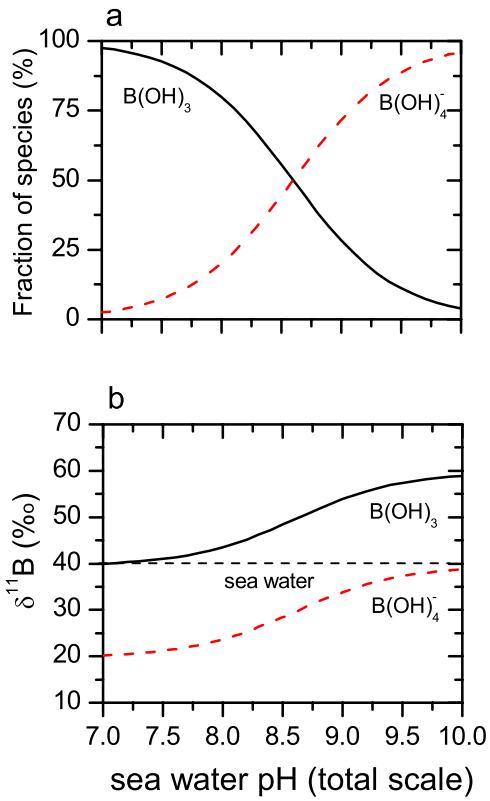

Figure 1. (a) Fraction and (b) isotopic composition of dissolved boron species as a function of pH. The curves are predicted under the condition of T = 25°C, S = 35 practical salinity units (psu), and $[B]_{tot}$ = 416 μmol/kg in the surface seawater.

2000], and in cultured shells of the planktic foraminifer *Orbulina universa* [*Sanyal et al.*, 1996], consistent with the model in which $B(OH)_4^-$ is adsorbed on the carbonate surface [*Hemming and Hanson*, 1992]. Values of K_D for B incorporation into these "marine carbonates" and inorganic calcite are roughly constant, at ~0.012 and 0.001, respectively [*Zeebe and Wolf-Gladrow*, 2001]. In contrast, K_D for B in *O. universa* is highly variable, with values ranging from 0.0003 to 0.0028. No clear relationship between B concentration and $\delta^{11}B$ was found in cultured or modern (core top) *Globigerinoides sacculifer* [*Sanyal et al.*, 1995; *Sanyal and Bijma*, 1999; *Sanyal et al.*, 2001]. However, a positive correlation between B/Ca and Mg/Ca (R^2 = 0.42, n = 15) in *G. sacculifer* from core Ocean Drilling Program (ODP) site 806 has been observed [*Wara et al.*, 2003], indicating that B incorporation in foraminifer shells may be influenced by their calcification temperature. Seawater pH decreases at higher temperatures, suggesting that B/Ca should decrease with increasing temperatures if pH is the only controlling factor. This pattern has been observed in corals, which show positive correlations between B/Ca and both Sr/Ca and U/Ca, the incorporation of which is inversely correlated with temperature [*Sinclair et al.*, 1998; *Fallon et al.*, 1999; *Sinclair*, 2005]. Ion microprobe analyses of B-doped calcite single crystals show that boron oxyanions are incorporated differently between nonequivalent vicinal faces [*Hemming et al.*, 1998], suggesting that, besides the fluid chemistry, crystal growth processes influence B incorporation into calcite.

[6] In this study, we have analyzed B/Ca ratios of core top planktonic foraminifera from the North Atlantic Ocean and the Southern Ocean to provide empirical calibrations for K_D in planktonic foraminifer shells. The temperature influence on K_D was also investigated using down core samples from the tropical Atlantic Ocean (ODP site 668B), for which independent pH estimates from boron isotopes are available [*Hönisch and Hemming*, 2005]. We estimated changes in aqueous pH and PCO_2 across termination I in the Southern Ocean, using B/Ca ratios of *Globorotalia inflata* from core CHAT 16K to assess the potential of B/Ca as a paleo-pH proxy.

2. Materials and Methods

2.1. Sediment Locations and Modern Hydrographic Data

[7] A suite of box core tops, collected between 35° and 65°N during the North East Atlantic Paleoceanography and Climate Change Project (NEAPACC) and Actuomicropaleontology Paleoceanography North Atlantic Project (APNAP) cruises in the North Atlantic (Table 1 and Figure 2) was used to investigate the variability of K_D into the planktonic foraminifera *Globigerina bulloides* and *Globorotalia inflata*. The core tops provide an ideal set of samples to investigate incorporation of trace elements into planktonic foraminifer shells and have been used for previous studies taking the advantage of systematic changes in surface water hydrography along the latitudinal transect [*Rickaby and Elderfield*, 1999; *Elderfield and Ganssen*, 2000; *Elderfield et al.*, 2000; *Barker and Elderfield*, 2002]. Because of thermodynamics, surface water temperature, pH, $[B(OH)_4^-/HCO_3^-]$ and $[CO_3^{2-}]$ increase from north to south and hence the latitudinal range serves as a good field to test B/Ca and variability of K_D. Radiocarbon dating verified that all core tops were <3 ka [*Rickaby and Elderfield*, 1999]. *G. inflata* of the late Holocene from ODP site 1088B and CHAT 16K in the Southern Ocean were analyzed to distinguish between temperature and carbonate ion (CO_3^{2-}) effects on K_D.

[8] The feasibility of using B/Ca as a paleo-pH proxy was tested directly by comparisons of foraminiferal B/Ca with a record of $\delta^{11}B$ from ODP site 668B (4°46′N, 20°55′W, 2693 m water depth) on the Sierra Leone Rise (Figure 2) [*Hönisch and Hemming*, 2005]. $\delta^{11}B$ data for ODP 668B were obtained using large *Globigerinoides sacculifer* (515–865 μm), but insufficient shells of this species were available for B/Ca. Therefore we analyzed B/Ca ratios in *Globigerinoides ruber* (w) (300–355 μm), which has a similar habitat depth as large *G. sacculifer* [*Spero et al.*, 2003]. *G. ruber* $\delta^{18}O$ data are from *Bird and Cali* [2002] and the chronology for ODP 668B is from *Hönisch and Hemming* [2005].

[9] B/Ca in *G. inflata* from core CHAT 16K (42°23.0′S, 178°29.9′W, 1408 m water depth) were measured across termination I (Figure 2). The core CHAT 16K is from the

Table 1. B/Ca Ratios in *G. inflata* and *G. bulloides* From Core Top Sediments[a]

				G. inflata						*G. bulloides*					
Core ID	Latitude, °N	Longitude, °W	WD, m	$\delta^{18}O_T$,[b] °C	T_{300m},[c] °C	$[CO_3^=]$,[c] μmol/kg	$[B(OH)_4^-/HCO_3^-]$,[c] mol/mol	B/Ca, μmol/mol	K_D, ×1000	$\delta^{18}O_T$,[b] °C	T_{50m},[c] °C	$[CO_3^=]$,[c] μmol/kg	$[B(OH)_4^-/HCO_3^-]$,[c] mol/mol	B/Ca, μmol/mol	K_D, ×1000
North Atlantic Ocean															
NEAP 2B	62.2	23.1	1268		7.4	156	0.0401	58	1.45						
NEAP 3B	61.5	23.1	1502		7.6	156	0.0401	58	1.44						
NEAP 4B	61.2	24.1	1627		7.7	157	0.0403	55	1.37						
NEAP 5B	61.0	24.3	1826		7.8	157	0.0404	58	1.44						
NEAP 7B	60.2	23.4	1997		8.1	157	0.0404	57	1.41						
NEAP 8B	59.4	22.1	2360		8.3	158	0.0405	54	1.33						
NEAP 10B	59.5	23.2	2221		8.3	158	0.0405	55	1.35						
NEAP 11B	59.5	22.4	2484		8.3	158	0.0405	52	1.28						
NEAP 13B	58.6	24.2	2546		8.6	159	0.0406	62	1.51						
NEAP 15B	57.4	25.4	2703		8.9	160	0.0408	59	1.45						
NEAP 17B	56.1	27.2	2734		9.1	161	0.0412	60	1.45						
NEAP 18B	54.4	28.2	2879								12.8	202	0.0517	42	0.81
NEAP 19B	52.5	30.2	3283		9.6	166	0.0423	59	1.39						
NEAP 20B	42.3	28.2	2878		12.0	173	0.0436	68	1.56		14.9	224	0.0568	50	0.88
T86 1B	53.4	27.5	2580	8.1	9.4	165	0.0420	69	1.65						
T86 3B	50.2	27.0	3113	9.4	10.0	171	0.0434	65	1.49						
T86 5B	46.9	25.4	3121	10.5	11.2	171	0.0433	69	1.60	13.7	13.4	212	0.0539	46	0.85
T86 8B	42.3	25.7	3232	12.0	12.0	173	0.0436	70	1.60	14.3	14.9	224	0.0568	44	0.77
T86 9B	40.8	27.5	2026	12.7	12.1	174	0.0437	71	1.63						
T86 10S	37.1	30.0	2610	14.5	12.5	179	0.0446	76	1.69						
T88 2B	57.9	26.0	2767	8.3	8.8	159	0.0407	62	1.52		11.5	194	0.0499	35	0.69
T88 3B	56.4	27.8	2819	7.0	9.1	161	0.0411	55	1.35						
T88 5B	53.6	27.1	2812	8.2	9.4	165	0.0420	70	1.66		12.8	203	0.0518	31	0.61
T88 6B	51.4	25.8	3381	9.4	9.7	169	0.0429	68	1.59						
T88 7B	50.5	26.5	3013	9.5	10.0	170	0.0434	75	1.72	11.8	12.9	205	0.0521	34	0.65
T88 9B	48.4	25.1	3074	10.8	10.6	172	0.0435	70	1.60	11.2	13.2	208	0.0529	46	0.88
T88 11B	45.4	25.4	2741	11.6	11.8	172	0.0434	72	1.66	15.2	13.6	211	0.0534	49	0.92
T88 12B	44.1	24.9	3052	11.6	12.0	172	0.0435	77	1.76	14.4	13.8	212	0.0539	50	0.93
T88 13B	42.9	25.3	3133	12.0	12.0	173	0.0436	76	1.74	14.4	14.3	218	0.0553	49	0.89
T88 14B	40.4	25.8	2858	12.1	12.1	174	0.0437	79	1.80						
T88 15aB	38.9	25.0	2738	13.2	12.1	175	0.0438	79	1.80						
T88 15B	38.6	25.0	2585	13.1	12.1	175	0.0438	75	1.71						
T90 1B	58.5	20.5	2911	8.2	8.6	159	0.0406	65	1.61						
T90 2B	53.1	20.8	2731	8.6	9.5	165	0.0421	66	1.56	10.2	12.9	204	0.0518	44	0.84
T90 3B	47.7	20.8	4479	10.5	10.9	171	0.0434	73	1.68						
T90 4B	47.2	21.4	3945	10.8	11.1	171	0.0433	75	1.73						
T90 5B	46.0	23.8	3069	10.6	11.5	171	0.0433	74	1.71	14.1	13.5	213	0.0544	36	0.66
T90 8B	46.2	23.7	3393	11.0	11.5	171	0.0433	73	1.69	14.3	13.5	213	0.0544	48	0.89
T90 11B	45.0	24.7	3208	11.4	11.9	172	0.0434	74	1.70	15.0	13.7	211	0.0536	49	0.91
T90 12B	40.6	20.1	5085		12.1	174	0.0437	74	1.69						
T90 15B	47.6	20.9	4177	10.5	10.9	171	0.0433	70	1.62						
Southern Ocean															
ODP 1088[d]	−41.1	−13.3	2082		11.5	148	0.0369	59	1.61						
CHAT 16K[e]	−42.4	178	1408		9.5	145	0.0366	58	1.58						

[a]Also shown are modern seawater temperature, $[CO_3^=]$, and $[B(OH)_4^-/HCO_3^-]$, estimated from the Global Ocean Data Analysis Project (GLODAP) data set for the species-specific habitat depths, and calculated K_D values. ODP is Ocean Drilling Program.
[b]$\delta^{18}O_T$ is calculated from $\delta^{18}O_{cc}$ and $\delta^{18}O_{sw}$ [*Elderfield and Ganssen*, 2000].
[c]Temperature, $[CO_3^=]$, and $[B(OH)_4^-/HCO_3^-]$ were estimated at 300 m for *G. inflata* and 50 m for *G. bulloides*.
[d]Samples picked from 2–4 cm.
[e]Samples picked from 0–1 cm.

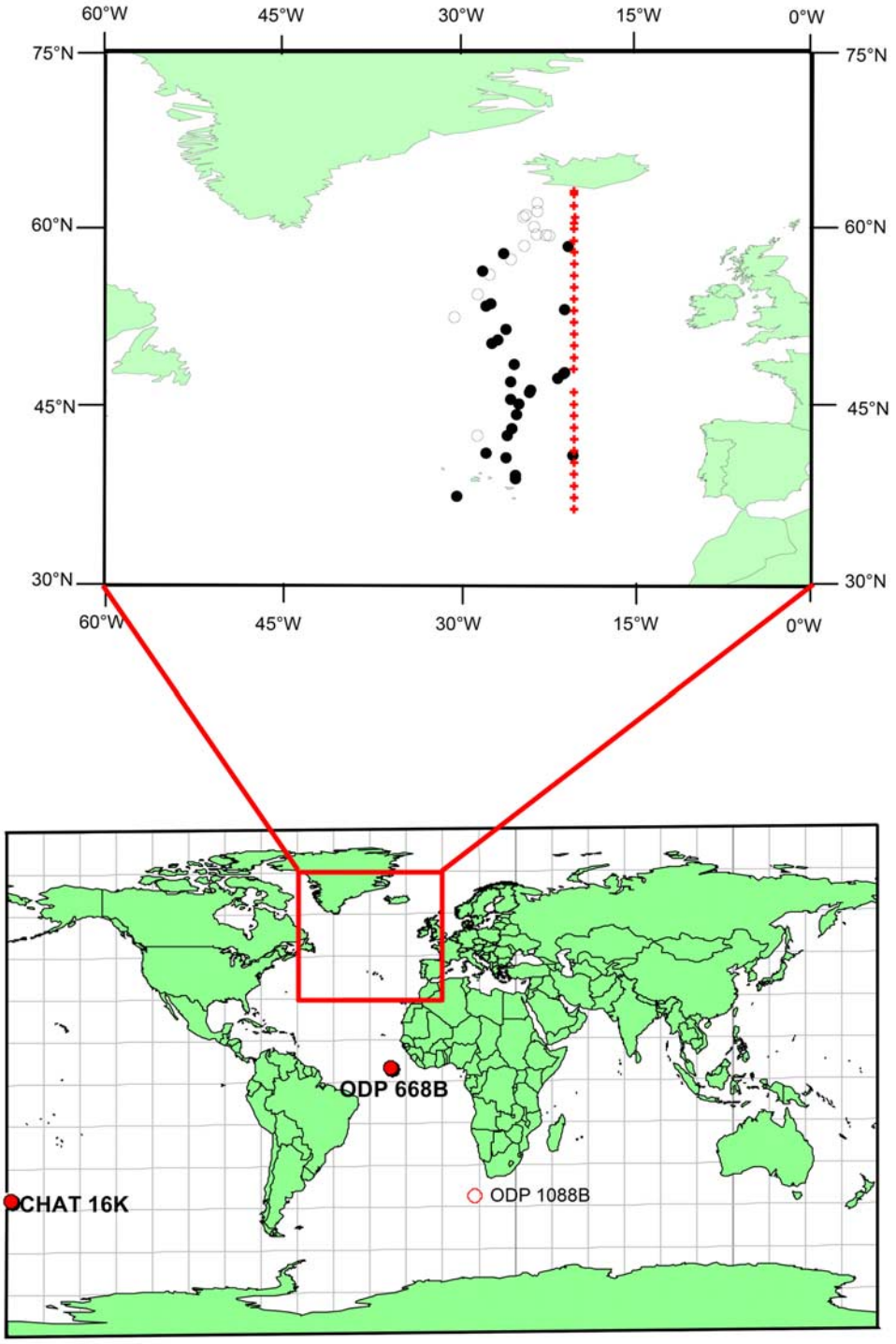

Figure 2. (top) Locations of box cores from the Actuomicropaleontology Paleoceanography North Atlantic Project (APNAP) (solid circles) and the NEAPACC (open circles) projects, as well as section 23 (crosses) of the Global Ocean Data Analysis Project (GLODAP) hydrographic data set. (bottom) Locations of Ocean Drilling Program (ODP) 1088B, ODP 668B, and CHAT 16K used in this study.

same location as core R657 studied by *Weaver et al.* [1997, 1998] and *Sikes et al.* [2002]. The CHAT 16K age model was constructed from benthic *Uvigerina spp*. $\delta^{18}O$ data (I.N. McCave, personal communication, 2006) and *G. inflata* $\delta^{18}O$ and Mg/Ca data are from *Greaves* [2007].

[10] For core top samples, modern hydrographic parameters including temperature, $[CO_3^{2-}]$, and $[B(OH)_4^-/HCO_3^-]$ in surface seawaters were estimated using the data set compiled by the Global Ocean Data Analysis Project (GLODAP) [*Key et al.*, 2004]. Section 23 was selected

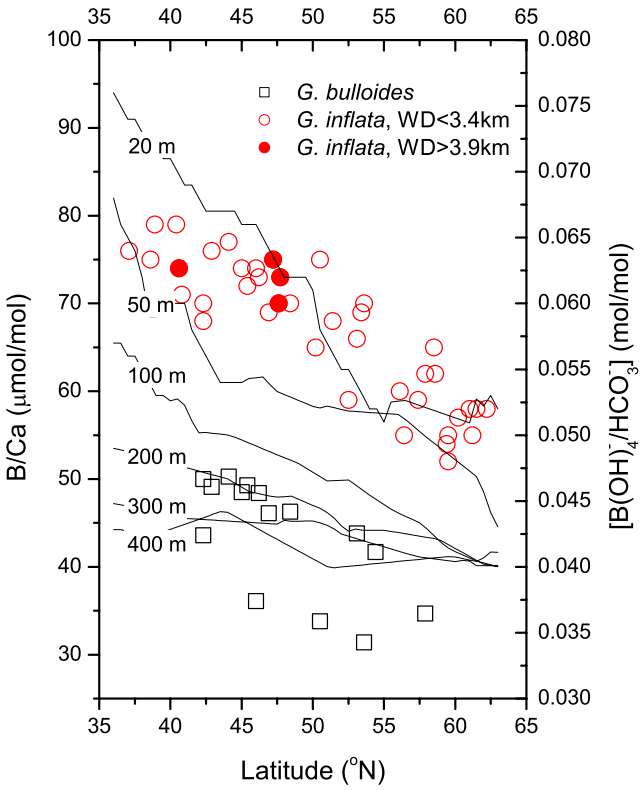

Figure 3. Core top B/Ca results of *G. bulloides* and *G. inflata* from the North Atlantic Ocean. Also shown are seawater $[B(OH)_4^-/HCO_3^-]$ (solid lines) at different water depths. The juxtaposition of the two ordinate scales is arbitrary.

for the core tops from the North Atlantic Ocean (Figure 2). We obtained total dissolved inorganic carbon (DIC), total alkalinity (ALK), together with nutrient levels (PO_4 and SiO_3), salinity (S), temperature, pressure (water depth) and anthropogenic CO_2 from the GLODAP hydrographic sites nearby the studied core top sites. The total boron concentration in seawater was calculated from S by $[B]_{tot}$ (μmol/kg) = 416 × S(practical salinity units (psu))/35 [*Uppstrom*, 1974]. The anthropogenic CO_2 contribution was subtracted from DIC, and the preindustrial concentrations of $B(OH)_4^-$, HCO_3^-, and CO_3^{2-} were calculated using CO_2sys.xls (version 12) [*Pelletier et al.*, 2005] (rewritten in VBA after CDIAC program version 1.05 [*Lewis and Wallace*, 1998]). We selected K_1 and K_2 according to *Mehrbach et al.* [1973] refit by *Dickson and Millero* [1987], K_B^* according to *DOE* [1994], and K_{SO4} according to *Dickson* [1990].

2.2. Analytical Methods

[11] Approximately 60–80 shells from each sample were picked from the 300–355 μm fraction and cleaned by two cleaning methods. Samples from core CHAT 16K were cleaned by the "Mg-cleaning" procedure [*Barker et al.*, 2003], while samples from other sites were cleaned by the "Cd-cleaning" method [*Boyle and Keigwin*, 1985/86; *Rosenthal et al.*, 1997]. Comparison of the two procedures showed a negligible effect on B/Ca ratios [*Yu*, 2006]. B/Ca and Mg/Ca ratios were analysed on the same solution by ICP-MS according to the method of *Yu et al.* [2005]. Measurements of B/Ca ratios are plagued both by high-B blanks from the introduction system and by a memory effect [*Al-Ammar et al.*, 1999; *Al-Ammar et al.*, 2000]. These difficulties were minimized by the use of a quartz spray chamber and by allocating longer washout and uptake times between measurements. Improvement has been made after the development of the method on ICP-MS [*Yu et al.*, 2005]. A new set of calibration standards was prepared to enlarge the B/Ca range to 0–260 μmol/mol. We used Milli-Q^+ to prepare the new standards and dissolution acid because Milli-Q^+ water has a lower boron concentration than quartz-distilled water (QD). The boron blank is <2% of the consistency standard (150 μmol/mol) and remains relatively stable during a typical run. The detection limit is ~10 μmol/mol. All samples and standards were run at 100 ppm [Ca] to avoid any possible matrix effect on B/Ca. The long-term precision over a 3-month period is 1.98% for B/Ca on the basis of replicate measurements of the consistency standard (n = 108). The majority of *G. inflata* from the North Atlantic core tops were analysed 2–3 times and results reported here are averages of the replicate measurements. On the basis of replicate measurements of standards and samples, the average precisions are <3.5% for B/Ca and <1.5% for Mg/Ca for results presented in this study.

3. Results

3.1. Core Top B/Ca

[12] In the North Atlantic Ocean, surface water temperature, $[B(OH)_4^-/HCO_3^-]_{seawater}$, $[CO_3^{2-}]$, and pH are highly correlated and increase with decreasing latitude (Table 1 and Figure 3). Similarly, *G. bulloides* and *G. inflata* show increasing B/Ca values with decreasing latitude, with *G. bulloides* displaying lower B/Ca ratios (30–50 μmol/mol) than *G. inflata* (50–80 μmol/mol) (Figure 3). Note that the juxtaposition of B/Ca and $[B(OH)_4^-/HCO_3^-]_{seawater}$ in Figure 3 is arbitrary. Lower B/Ca ratios in *G. bulloides* are unexpected because this species lives in shallower, more alkaline water depth relative to *G. inflata*. The trend of B/Ca in *G. bulloides* is more scattered, presumably due to the difficulty of measuring low B/Ca ratios. *G. inflata* from sites with different ranges of water depth (>3.9 km and <3.4 km) display a single evolution trend along the transect. Core top samples of *G. inflata* from ODP 1088B and CHAT 16K have B/Ca ratios of ~60 μmol/mol, i.e., within the range of the North Atlantic core tops (Table 1). However, because of higher nutrient levels in the Southern Ocean the estimated $[CO_3^{2-}]$ (~145 μmol/kg) for these two cores are lower relative to those for core tops from the North Atlantic Ocean (155–175 μmol/kg).

[13] The B/Ca ratios in *G. bulloides* and *G. inflata* are lower than those in the marine carbonates (90–650 μmol/mol) analyzed by *Hemming and Hanson* [1992] and corals (400–600 μmol/mol) [*Sinclair et al.*, 1998; *Fallon et al.*, 1999; *Sinclair*, 2005], but similar to values in cultured *O. universa* (60–80 μmol/mol) [*Sanyal et al.*, 1996] and those in core top *G. sacculifer* (90–140 μmol/mol) [*Sanyal et al.*, 1995].

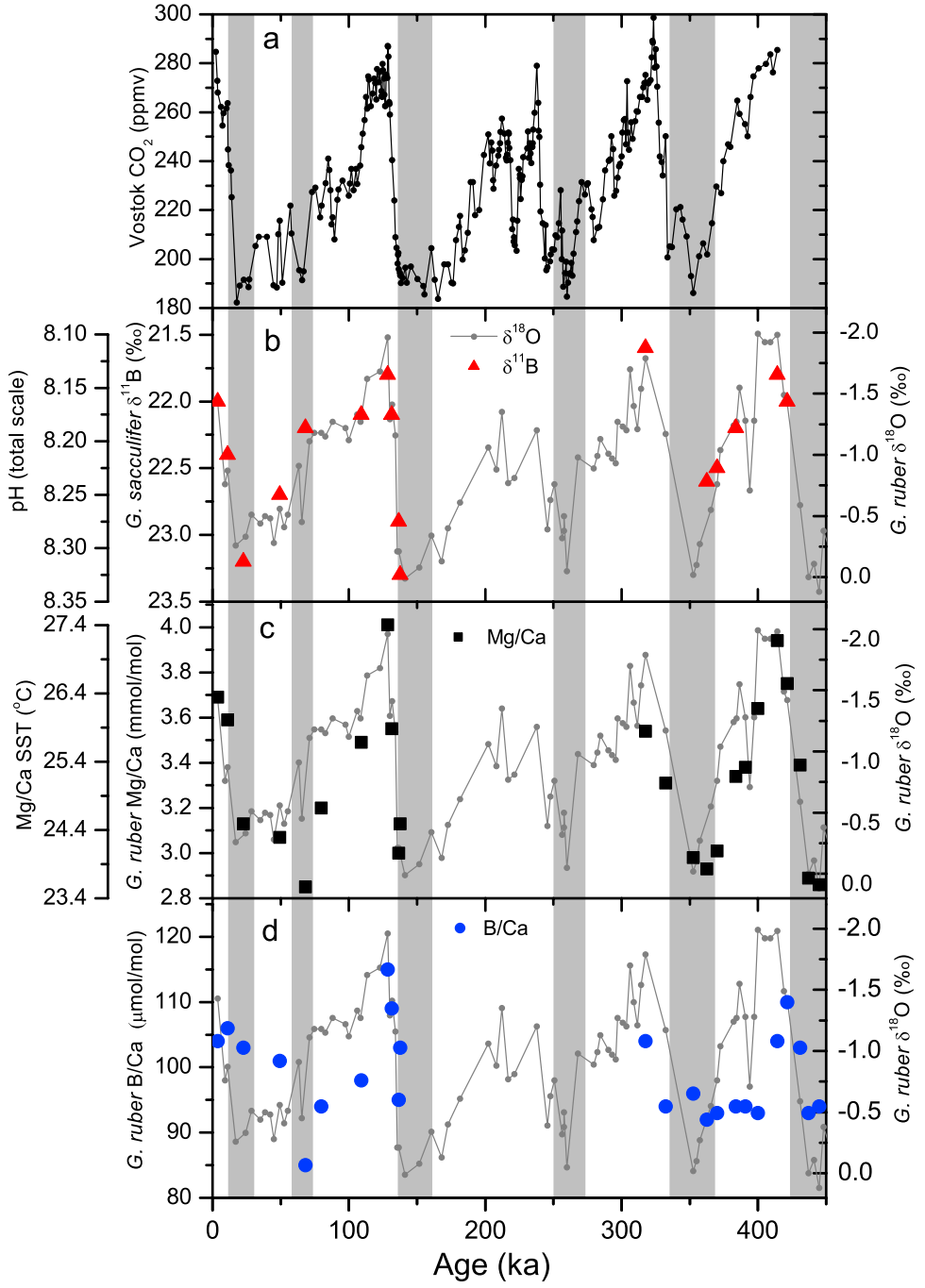

Figure 4. Atmospheric pCO_2 from the Vostok ice core [*Petit et al.*, 1999] (a), $\delta^{11}B$ in *G. sacculifer* [*Hönisch and Hemming*, 2005] (b), Mg/Ca (c), and B/Ca (d) of *G. ruber* (w) (this study) from ODP 668B. Also plotted are *G. ruber* $\delta^{18}O$ (continuous record in gray) in Figures 4b–4d. Grey bars indicate glacial intervals.

3.2. ODP 668B

[14] The $\delta^{11}B$ results in *G. sacculifer* from ODP 668B indicate that sea surface PCO_2 and atmospheric pCO_2 at this site have been in equilibrium over the past ~400 ka (Figures 4a and 4b) [*Hönisch and Hemming*, 2005]. Mg/Ca ratios are high during interglacial intervals and low during glacial intervals; and show an inverse correlation with $\delta^{18}O_{G.\ ruber(w)}$ (Figure 4c and Table 2). Sea surface temperature (SST) was obtained from Mg/Ca ratios using the calibration of *Anand et al.* [2003], with the preexponential coefficient adjusted to 0.34 to match core top values to the modern value. Calculated values of SST are consistent with those from *Hönisch and Hemming* [2005], showing a ~3°C change in temperature between full glacial and

Table 2. Foraminiferal B/Ca and Mg/Ca Ratios in *G. ruber* (w) From ODP 668B Together With Calculated $[B(OH)_4^-/HCO_3^-]$, $[CO_3^{2-}]$, and K_D Values Using Two Models Given in *Hönisch and Hemming* [2005][a]

Core Section, Interval	Age,[b] Vostok Gas Age Scale	B/Ca *G. ruber* (w), μmol/mol	Mg/Ca *G. ruber* (w), mmol/mol	Mg-SST,[c] °C	Model 1			Model 2			Model 1[d]		Model 2[d]	
					$[B(OH)_4^-/HCO_3^-]$, mol/mol	$[CO_3^{=}]$, μmol/kg	K_D, ×1000	$[B(OH)_4^-/HCO_3^-]$, mol/mol	$[CO_3^{=}]$, μmol/kg	K_D, ×1000	pH, total scale	PCO_2, μatm	pH, total scale	PCO_2, μatm
1-1, 2–4 cm	3833	104	3.69	26.5	0.0731	311	1.43	0.0710	287	1.47	8.15	306	8.16	289
1-1, 25–27 cm	11013	106	3.59	26.2	0.0784	332	1.35	0.0759	304	1.39	8.18	289	8.19	270
1-1, 33–35 cm	22723	103	3.13	24.7	0.0987	359	1.04	0.0996	367	1.03	8.28	207	8.27	213
1-1, 70–72 cm	49414	101	3.07	24.5	0.0839	330	1.20	0.0833	323	1.21	8.28	208	8.28	205
1-1, 105–107 cm	68107	85	2.85	23.6	0.0730	273	1.16	0.0758	303	1.12	8.28	197	8.27	216
1-1, 125–127 cm	79837	94	3.20	24.9							8.23	236	8.22	243
1-2, 25–27 cm	109163	98	3.49	25.9	0.0705	278	1.39	0.0717	292	1.37	8.19	265	8.18	279
1-2, 39–41 cm	128399	115	4.01	27.4	0.0650	273	1.77	0.0648	270	1.78	8.14	303	8.14	305
1-2, 49–51 cm	131320	109	3.55	26.0	0.0688	283	1.58	0.0687	282	1.58	8.21	251	8.21	252
1-2, 70–72 cm	136632	95	3.00	24.2	0.0903	337	1.05	0.0916	349	1.04	8.28	206	8.27	214
1-2, 74–76 cm	137694	103	3.13	24.7	0.0959	366	1.07	0.0951	358	1.08	8.27	216	8.27	212
2-2, 56–58 cm	317445	104	3.54	26.0	0.0655	259	1.58	0.0669	276	1.55	8.20	249	8.19	267
2-2, 75–77 cm	332293	94	3.31	25.3							8.19	278	8.20	257
2-2, 85–87 cm	352412	96	2.98	24.1							8.27	223	8.28	205
2-2, 105–107 cm	362425	92	2.93	23.9	0.0858	344	1.07	0.0837	322	1.10	8.27	218	8.28	206
2-2, 130–132 cm	370031	93	3.01	24.2	0.0794	317	1.17	0.0786	308	1.18	8.26	219	8.27	214
2-3, 14–16 cm	383734	94	3.34	25.4	0.0746	303	1.26	0.0739	295	1.27	8.19	271	8.19	266
2-3, 25–27 cm	390865	94	3.38	25.5							8.17	285	8.18	273
2-3, 39–41 cm	399940	93	3.64	26.4							8.13	311	8.12	325
2-3, 56–58 cm	414085	104	3.94	27.2	0.0674	276	1.54	0.0676	278	1.54	8.11	329	8.11	336
2-3, 70–72 cm	421574	110	3.75	26.7	0.0716	291	1.53	0.0718	293	1.53	8.17	280	8.17	285
2-3, 77–79 cm	430869	103	3.39	25.5							8.21	251	8.21	252
2-3, 85–87 cm	437094	93	2.89	23.8							8.29	204	8.29	201
2-3, 95–97 cm	444875	94	2.86	23.7							8.30	200	8.30	195

[a]Also shown are paleo-pH and PCO_2 estimated from B/Ca. Model 1 uses the deconvolution of foraminiferal $\delta^{18}O$ and Mg/Ca to yield local salinity, while model 2 uses the theoretical concentration of salt due to changing sea level.
[b]From *Hönisch and Hemming* [2005].
[c]Mg-SST calculated by: SST = LN[(Mg/Ca)/0.34]/0.09 after *Anand et al.* [2003].
[d]The pH and PCO_2 calculated from B/Ca.

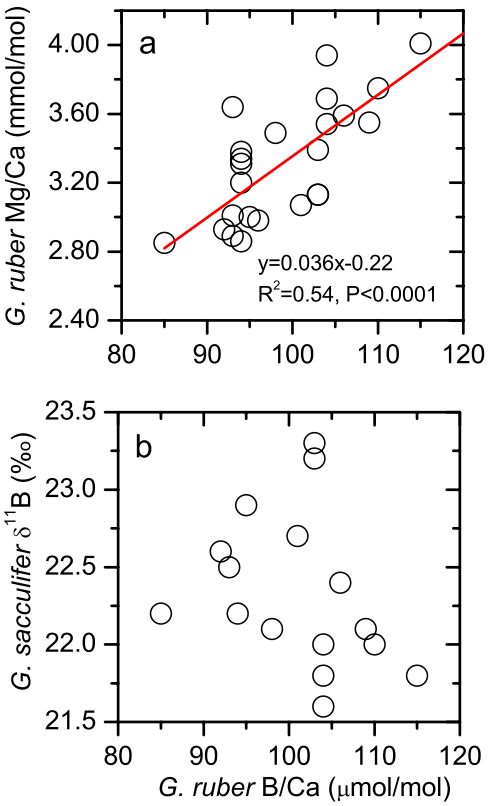

Figure 5. (a) B/Ca versus Mg/Ca and (b) B/Ca versus δ^{11}B for samples from ODP 668B. B/Ca is positively correlated with Mg/Ca, but no significant relationship exists between B/Ca and δ^{11}B.

interglacial intervals. We used the newly measured Mg/Ca data because Mg/Ca and B/Ca ratios were obtained on the same solutions. B/Ca in *G. ruber* (w) from ODP 668B ranges between 85–115 μmol/mol (Figure 4d), similar to that recorded in *G. sacculifer* [*Sanyal et al.*, 1995]. There is no correlation between B/Ca and δ^{11}B (R^2 = 0.10, P = 0.28, n = 16), but B/Ca and Mg/Ca show a positive correlation (R^2 = 0.54, P < 0.0001, n = 24) (Figure 5).

3.3. CHAT 16K

[15] B/Ca ratios in *G. inflata* across termination I range between 50–70 μmol/mol, without any significant difference between glacial and interglacial intervals (Table 3 and Figure 6a). Mg/Ca ratios show the lowest values at the Last Glacial Maximum (LGM) and the highest ratios in the early Holocene, inversely correlated with δ^{18}O (Figures 6b and 6c). Conversion of Mg/Ca to temperature, using the equation from *Mashiotta et al.* [1999] (Mg/Ca = 0.474exp[0.107SST]), indicates a ~3°C warming across termination I. No clear correlation is found between B/Ca and Mg/Ca (R^2 = 0.001, P = 0.85, n = 30) or δ^{18}O (R^2 = 0.04, P = 0.26, n = 31) for CHAT 16K.

4. Discussion

4.1. Dissolution and Vital Effects on B/Ca

[16] Dissolution may lower element/Ca (e.g., Mg/Ca) ratios in foraminifera [*Rosenthal and Boyle*, 1993; *Brown and Elderfield*, 1996]. Examination of core top sample T90-12B (water depth = 5058 m) revealed that shells of *G. bulloides* are thinned and broken and the shell weight of *G. inflata* from this sample is significantly lower compared with nearby shallower sites [*Barker*, 2002], indicating partial dissolution of foraminiferal tests. However, B/Ca in *G. inflata* from water depths greater than 3.9 km show no deviation from the trend defined by samples from shallower sites of our North Atlantic transect study (Figure 3). No correlation between B/Ca and deep water $\Delta[CO_3^{2-}]$ is observed for core top samples (Figure 7). *Wara et al.* [2003] also found a negative correlation between their down-core B/Ca and shell weight data for *G. sacculifer* from ODP site 806. Therefore it appears that dissolution has little effect on B/Ca in planktonic foraminifera.

[17] Different ranges exist in B/Ca ratios between species. Possible causes of B/Ca differences between species comprise kinetic effects (such as growth rate), modification of ambient seawater chemistry by physiological processes (such as symbiont photosynthesis, respiration, and calcification), and microenvironments within organisms nucleating calcium carbonate. Our study shows that symbiont-bearing species, *G. ruber* (w), have higher B/Ca ratios than symbiont-barren species *G. bulloides* and *G. inflata* (Figures 3 and 4d). Previous model and experimental studies show that microenvironmental pH surrounding symbiont-bearing species is elevated under highlight conditions [*Wolf-Gladrow et al.*, 1999; *Zeebe et al.*, 2003; *Hönisch et al.*, 2003]. It is possible that these "vital effects" may vary between specimens of the same species, as suggested by different Mg/Ca and Sr/Ca ratios between different size fractions of the same planktonics species [*Elderfield et al.*, 2002]. Although we have not tested this potential complication, we restricted our samples to a narrow size range (300–355 μm) and used large number of shells (60–80 tests) for each sample to minimize size variations caused by sieving.

4.2. Estimation of K_D

[18] The increase of foraminiferal B/Ca with decreasing latitude is to be expected from equation (3) because $[B(OH)_4^-/HCO_3^-]_{seawater}$ ratios are higher at warmer, lower latitudes in the North Atlantic Ocean (Figure 3). K_D values were calculated for the core top planktonic foraminifera by combining measured B/Ca with local $[B(OH)_4^-/HCO_3^-]_{seawater}$ estimated from the GLODAP data set on the basis of habitat depths of *G. bulloides* and *G. inflata* in the North Atlantic Ocean. Planktonic foraminifera are thought to migrate vertically throughout their development and shell abundances are affected by size, seasonal and interannual variability, regional water structure and food availability [*Bé*, 1977; *Erez and Honjo*, 1981; *Fairbanks et al.*, 1982; *Deuser and Ross*, 1989; *Ganssen and Kroon*, 2000]. Most studies indicate that *G. bulloides* mainly calcifies in the surface mixed layer (~50 m) [*Fairbanks et al.*, 1982; *Ganssen and Kroon*, 2000; *Anand et al.*, 2003] while *G. inflata* prefers to grow in deeper waters and average habitat depths vary at different locations in the Atlantic Ocean [*Mortyn and Charles*, 2003; *Anand et al.*, 2003; *Wilke et al.*, 2006; *Lončarić et al.*, 2006]. In the

Table 3. The $\delta^{18}O$, Mg/Ca, and B/Ca Data of *G. inflata* From CHAT 16K Across Termination I Together With Calculated Temperature, pH, and PCO_2 Values

Depth, cm	Age,[a] ka	$\delta^{18}O$, ‰, PDB	Mg/Ca, mmol/mol	B/Ca, μmol/mol	Mg-SST,[b] °C	pH,[c] Total Scale	PCO_2,[c] μatm	pH,[d] Total Scale	PCO_2,[d] μatm
0	0.00	1.68	1.27	58	9.20	8.11	321	8.12	318
2	1.31	2.27	1.26	56	9.17	8.09	348	8.10	332
4	2.63	1.25	1.35	53	9.79	8.06	365	8.06	371
6	3.94	1.96	1.35	53	9.80	8.05	387	8.06	374
8	5.26	2.11	1.10	54	7.87	8.12	310	8.13	308
10	6.57	2.64	1.31	59	9.48	8.10	344	8.12	322
12	7.89	3.34	1.30	57	9.43	8.07	380	8.11	339
14	9.20	2.22	1.43	61	10.31	8.09	352	8.11	334
16	10.51	2.45	1.37	62	9.93	8.11	335	8.13	314
18	11.83	3.08	1.28	57	9.26	8.08	367	8.11	333
20	13.14	4.26	1.02	58	7.15	8.15	308	8.19	270
22	14.14	3.65	1.10	55	7.86	8.11	340	8.15	304
24	14.83	3.53	0.88	57	5.82	8.21	254	8.23	237
26	15.52	3.48	0.98	56	6.83	8.16	289	8.19	267
28	16.21	3.59	0.97	62	6.67	8.21	256	8.24	234
30	16.90	3.43	1.15	59	8.27	8.13	321	8.16	292
32	17.59	3.53	0.94	59	6.35	8.20	262	8.22	244
34	18.28	3.32	1.05	68	7.42	8.23	242	8.25	224
36	18.97	3.63	0.93	62	6.28	8.22	246	8.25	226
38	19.66	3.52	0.97	58	6.70	8.18	274	8.21	254
41	20.69	3.48	0.93	61	6.32	8.22	248	8.24	229
45	22.07	3.93	0.97	60	6.65	8.19	273	8.23	245
49	23.44	3.46		60					
53	24.82	3.61	0.91	54	6.14	8.17	285	8.20	263
57	26.20	3.40	0.97	61	6.70	8.20	257	8.23	238
61	27.33	3.59	0.93	56	6.30	8.18	277	8.20	257
65	28.46	3.47	0.95	53	6.49	8.15	300	8.17	278
69	29.59	3.18	1.11	58	7.92	8.14	310	8.16	286
73	30.72	2.98	1.22	63	8.84	8.14	306	8.17	282
77	31.86	2.83	1.25	62	9.10	8.13	318	8.15	295
81	32.99	2.28	1.23	61	8.90	8.14	303	8.15	291

[a]After I. N. McCave, personal communication, 2006.
[b]Calculated according to *Mashiotta et al.* [1999].
[c]Calculated assuming $[B]_{tot}$ changing with salinity.
[d]Calculated assuming a constant $[B]_{tot}$ of 410 μmol/kg.

Southern Atlantic, *G. inflata* shows the highest shell abundance at 300–500 m at TNO57-21 (42°S, 8°E), but further south (43°S–53°S) the calcification depth of this species appears to be shallower (~100 m) because of differences in hydrography [*Mortyn and Charles*, 2003]. Using an oxygen isotope mass balance model, plankton tow results along the SW African continental margin (29–33°S) show that *G. inflata* calcifies between 0 and 500 m, but the mass development patterns are different at four studied sites [*Wilke et al.*, 2006]. Deep tow and sediment trap results at central Walvis Ridge (27°S) show that *G. inflata* record the temperature between 150 and 350 m, and coarse fractions display a deeper shell concentration than fine fractions [*Lončarić et al.*, 2006]. In the Sargasso Sea (32°N), sediment trap study indicates an apparent calcification depth of *G. inflata* of 100–400 m [*Anand et al.*, 2003]. We cannot carry out the methodology laid out in *Wilke et al.* [2006] and there is no means to reconstruct mass accumulation patterns for paleosamples. Therefore we have estimated $[B(OH)_4^-/HCO_3^-]_{seawater}$ at average habitat depths for *G. bulloides* and *G. inflata* on the basis of comparison of $\delta^{18}O$ calcification temperature and GLODAP temperature [*Elderfield and Ganssen*, 2000; *Key et al.*, 2004]. This comparison indicates that *G. bulloides* and *G. inflata* calcified their shells at average depths of ~50 and ~300 m, respectively (Table 1). Therefore $[B(OH)_4^-/HCO_3^-]_{seawater}$ estimated at 50 and 300 m reasonably represent the average hydrographic conditions experienced during the ontogeny of *G. bulloides* and *G. inflata* at the core top sites. However, it must be stressed that the assumption that any particular species represents a strict depth horizon is an oversimplification and the choice of different habitat depths as well as consideration of seasonality of foraminiferal growth will affect $[B(OH)_4^-/HCO_3^-]_{seawater}$ and hence K_D values. To explore these effects, we estimated uncertainties of $[B(OH)_4^-/HCO_3^-]_{seawater}$ and K_D values by assigning habitat depths of 30–70 m for *G. bulloides* and 250–350 m for *G. inflata*.

[19] The estimation of K_D for *G. ruber* (w) from ODP site 668B is more complex because $[B(OH)_4^-]$ and $[HCO_3^-]$ of past seawater are unknown. To calculate $[B(OH)_4^-/HCO_3^-]_{seawater}$ and thus quantify K_D, we used pH derived from $\delta^{11}B$ of *G. sacculifer*, SST derived from Mg/Ca in *G. ruber* (w), together with ALK and $[B]_{tot}$ values estimated from salinity. Because of its secretion of gametogenic calcite at depth, *G. sacculifer* has a slightly deeper habitat depth (~75 vs. ~25 m) than *G. ruber* (w) and $\delta^{11}B$ in *G. sacculifer* would reflect a depth-integrated pH value, which is not exactly the same as that for *G. ruber* (w).

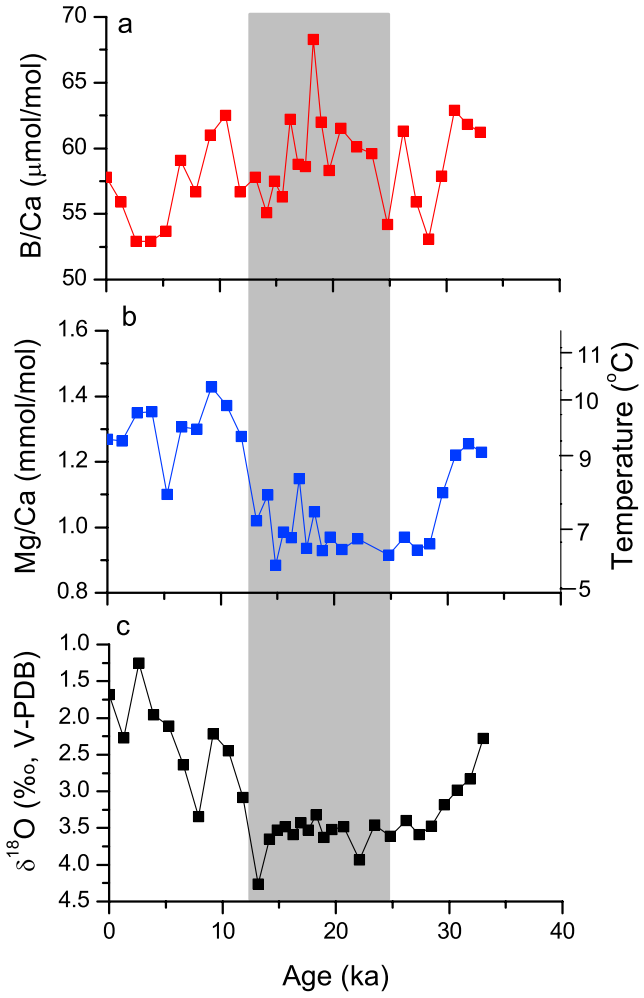

Figure 6. (a) B/Ca, (b) Mg/Ca, and (c) δ^{18}O in *G. inflata* across termination I from CHAT 16K in the Southern Ocean. The gray bar indicates Marine Isotope Stage (MIS) 2.

However, large pH gradients are not expected in the mixed surface water. Modern hydrographic data show that the thickness of the mixed layer is ~70 m at ODP 668B [*Key et al.*, 2004]. Previous studies also suggest that larger *G. sacculifer* shells, which were used for δ^{11}B measurements at ODP 668B [*Hönisch and Hemming*, 2005], appear to live warmer and shallower environments relative to smaller individuals [*Spero et al.*, 2003; *Hönisch and Hemming*, 2004]. Therefore pH calculated from δ^{11}B in *G. sacculifer* provide the first approximation for the ambient pH recorded in *G. ruber*. The uncertainties introduced by this approach seem to be insignificant because of mixing in the surface seawater and equilibrium between surface water and atmosphere suggested by *G. sacculifer* δ^{11}B results for the past 400 kyr [*Hönisch and Hemming*, 2005]. Following the approach given in *Hönisch and Hemming* [2005], two models were used to estimate changes in ALK and $[B]_{tot}$. In the first model the local salinity was calculated from $\delta^{18}O_{cc}$, $SST_{Mg/Ca}$, and the local S-$\delta^{18}O_{sw}$ relationship ($\delta^{18}O_{sw}$ = 0.20 × S − 6.73, R^2 = 0.61). In the second model, salinity variations were estimated using the global sea level change. In both models, ALK was calculated by ALK = 65.62 × S + 22.84 (R^2 = 0.57) [*Hönisch and Hemming*, 2005], and $[B]_{tot}$ was calculated using $[B]_{tot}$ (μmol/kg) = 416 × S/35 [*Uppstrom*, 1974].

[20] As shown in equation (3), foraminiferal B/Ca is a function of K_D and $[B(OH)_4^-/HCO_3^-]_{seawater}$. Therefore a plot of B/Ca vs. $[B(OH)_4^-/HCO_3^-]_{seawater}$ defines lines of constant K_D with which to compare core top and down-core data (Figure 8). B/Ca values in core top *G. bulloides* and *G. inflata* from the North Atlantic are positively correlated with $[B(OH)_4^-/HCO_3^-]_{seawater}$, indicating a seawater pH influence on incorporation of B into carbonates [*Hobbs and Reardon*, 1999]. Taking account of uncertainties associated with B/Ca and $[B(OH)_4^-/HCO_3^-]_{seawater}$, neither regression lines passes through the origin, showing that K_D is variable within each species. Core top *G. inflata* samples from the Southern Ocean have higher B/Ca ratios as compared with the trend defined by the North Atlantic core tops. In contrast to the core top samples, B/Ca in *G. ruber* (w) from ODP 668B decrease with increasing $[B(OH)_4^-/HCO_3^-]_{seawater}$. Assigning different habitat depths (*G. ruber*: 0–50 m, *G. bulloides*: 30–70 m, and *G. inflata*: 250–350 m) and using different models for estimating salinity in samples from ODP 668B would slightly change absolute $[B(OH)_4^-/HCO_3^-]_{seawater}$ and K_D values, but their variability would not be affected. The K_D ranges observed are (Figure 8): 0.0006–0.0009 (50% variability) for *G. bulloides*, 0.0013–0.0018 (40% variability) for *G. inflata*, and 0.0010–0.0018

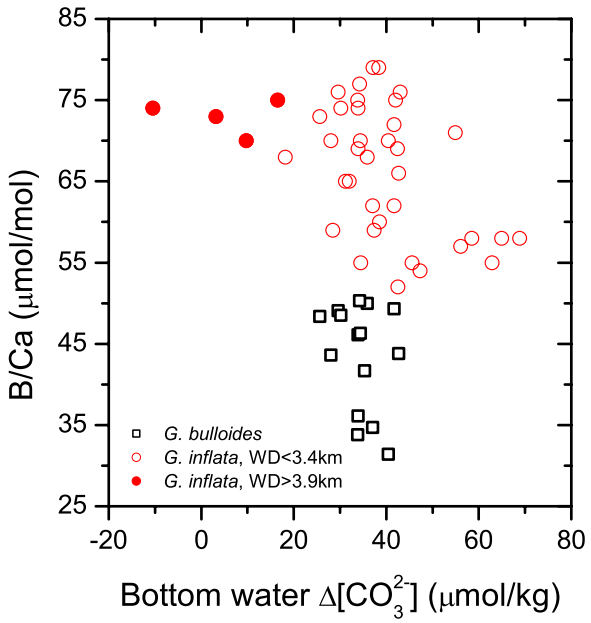

Figure 7. Cross plot of B/Ca versus bottom water calcite saturation $\Delta[CO_3^{2-}]$ for North Atlantic core tops to demonstrate little dissolution effect on B/Ca. Bottom water $\Delta[CO_3^{2-}]$ values were calculated using the GLODAP data set [*Key et al.*, 2004] and CO_2sys.xls (version 12) [*Pelletier et al.*, 2005].

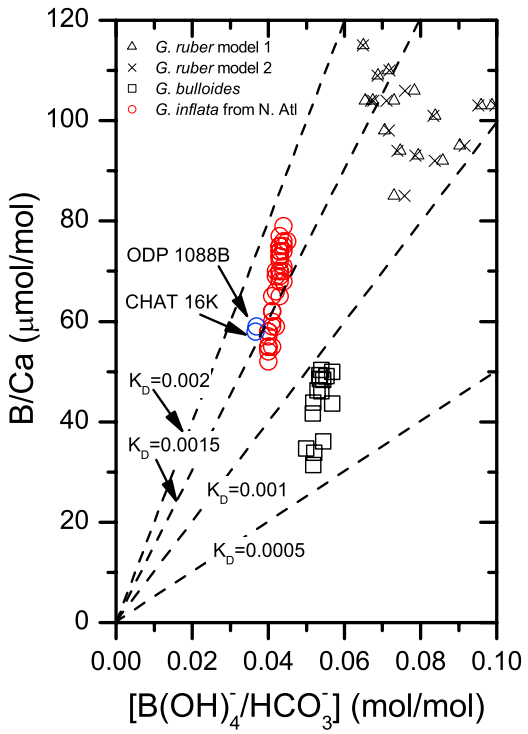

Figure 8. Foraminiferal B/Ca versus seawater $[B(OH)_4^-/HCO_3^-]$. The relative uncertainty of the species-specific habitat depth (*G. ruber*: 0–50 m, *G. bulloides*: 30–70 m, and *G. inflata*: 250–350 m) translates into uncertainties on $[B(OH)_4^-/HCO_3^-]$ that are no larger than the symbol sizes. *G. bulloides* and *G. inflata* display linear B/Ca-$[B(OH)_4^-/HCO_3^-]$ relationships, where B/Ca in *G. ruber* (w) shows no significant correlation with $[B(OH)_4^-/HCO_3^-]$. Note that B/Ca in *G. inflata* from Southern Ocean cores ODP 1088B and CHAT 16K deviate from the North Atlantic trend.

(80% variability) for *G. ruber* (w). We conclude that seawater pH ($[B(OH)_4^-/HCO_3^-]$) cannot be estimated from B/Ca in planktonic foraminifera via a constant K_D.

4.3. Effect of Temperature on K_D

[21] At a constant temperature, K_D into inorganic calcites precipitated in the laboratory shows a constant value of ~0.001 and it appears that B/Ca ratios in such samples are dominantly determined by fluid pH [*Sanyal et al.*, 2000]. On the basis of a positive correlation between B/Ca and Mg/Ca in *G. sacculifer* from ODP site 806, *Wara et al.* [2003] suggested that calcification temperature may exert an influence on B concentration in planktonic foraminifera. Similarly, B/Ca ratios in *G. ruber* (w) from ODP site 668B increase with increasing Mg/Ca (Figure 5a). Core top *G. inflata* from the Southern Ocean have higher B/Ca than extrapolation of the North Atlantic data to their $[B(OH)_4^-/HCO_3^-]_{seawater}$ would predict and calcified at warmer temperatures than their North Atlantic counterparts (Figure 7 and Table 1). Comparison of K_D and calcification temperature for the species studied supports a temperature dependence of K_D (Figure 9a). The K_D for *G. ruber* (w) shows a temperature sensitivity of 13% change per °C (R^2 = 0.83, n = 16) and that for *G. inflata* a 5% change per °C (R^2 = 0.65, n = 40). The correlation for *G. bulloides* is not significant (R^2 = 0.20, n = 15), perhaps a reflection of the

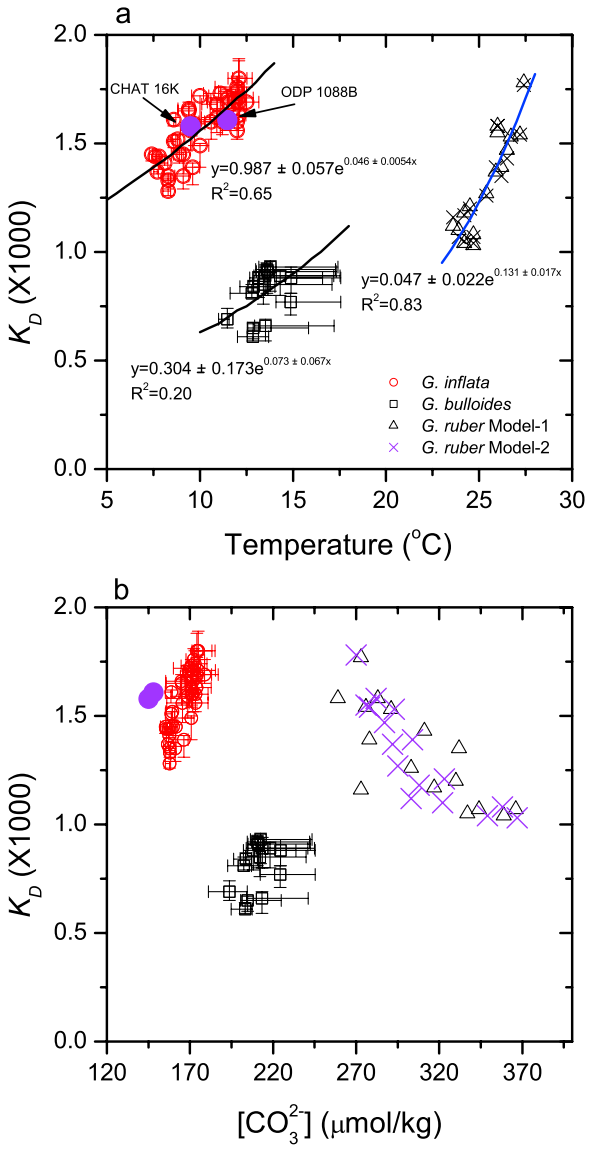

Figure 9. Variations of K_D with temperature (a) and $[CO_3^{2-}]$ (b) for three planktonic foraminifer species. Error bars for core top samples of *G. bulloides* and *G. inflata* are estimated assuming habitat depths of 30–70 m and 250–350 m, respectively. For *G. ruber* (w) from ODP 668B, $[CO_3^{2-}]$ and K_D values are calculated by two models using $\delta^{11}B$ data and an assumed alkalinity. It is assumed that *G. ruber* (w) live in the surface (40 m), but use of different depths (0–50 m) has insignificant influences on calculated variables. Data were fitted to an exponential model because linear regressions would imply zero K_D at a range of temperatures. Also shown in Figure 9a are 95% confidence uncertainties associated with preexponential and exponential constants.

scatter in data because of the low B/Ca ratios (Figure 3). Temperatures estimated from the GLODAP data set are used in Figure 9a because $\delta^{18}O_T$ data for the samples are incomplete (Table 1) [*Key et al.*, 2004]. Our results indicate that B/Ca ratios in planktonic foraminifera are affected by temperature in addition to pH, but K_D can be estimated using the temperature dependencies displayed in Figure 9a.

[22] The actual mechanism of B incorporation into foraminiferal calcite is not well understood and thus we can only speculate on the reason for the temperature effect. Boron occurs predominantly in trigonal coordination in foraminiferal calcite and the incorporation of B into $CaCO_3$ requires a transition from the tetrahedral structure of the adsorbed $B(OH)_4^-$ to the trigonal coordination [*Hemming et al.*, 1998; *Zeebe and Wolf-Gladrow*, 2001]. If the transition rate increases with temperature, higher B/Ca ratios in $CaCO_3$ would be expected at higher temperatures. In contrast to inorganic calcites, the precipitation of biogenic carbonates is heavily mediated by biological processes, and the temperature dependence of K_D may be explained in terms of the microenvironments within which foraminifera nucleate calcium carbonate. *Elderfield et al.* [1996] proposed that foraminifera calcify their tests from an internal reservoir rather than directly from the ambient seawater. If the flushing rate increases with temperature, the degree of calcification, a process that produces CO_2 and hence decreases pH, of the internal pool would be lower at higher temperatures. Therefore the enhanced carbon utilization at lower temperatures would decrease the pH of the internal biomineralization reservoir and this would eventually lead to less boron being incorporated into the calcite. For *G. ruber* (w), the pH of the ambient seawater may also be modified through symbiont processes which may vary with the temperature.

4.4. Caveats

[23] It has been documented that $[CO_3^{2-}]$ may have significant effects on foraminiferal $\delta^{18}O$, $\delta^{13}C$, and some metal/Ca ratios (e.g., Zn/Ca and U/Ca) [*Spero et al.*, 1997; *Marchitto et al.*, 2000; *Russell et al.*, 2004]. Surface water temperature and $[CO_3^{2-}]$ change in unison in the North Atlantic Ocean [*Barker and Elderfield*, 2002]. Therefore we have also considered whether changes in K_D might instead be described in terms of changes in $[CO_3^{2-}]$. Core top *G. inflata* from the North Atlantic show a clear correlation between K_D and $[CO_3^{2-}]$ (Figure 9b). However, *G. inflata* from the Southern Ocean do not fall along the trend defined by the North Atlantic samples (Figure 9b). Because temperature and $[CO_3^{2-}]$ are inversely correlated in ODP 668B, *G. ruber* (w) show a negative relationship between K_D and $[CO_3^{2-}]$, which is inconsistent with the correlation observed for *G. inflata*. Therefore a control of CO_3^{2-}rather than temperature on K_D is unsupported by the data. Similarly, it is unlikely that K_D into planktonic foraminifera is controlled by salinity.

[24] We used the GLODAP data set to estimate seawater temperature and $[B(OH)_4^-/HCO_3^-]$ which may not represent exact conditions under which foraminiferal shells were calcified. Hydrographic data of section 23 used for core tops from the North Atlantic were measured in the summer (July and August 1993) [*Key et al.*, 2004]. Generally, *G. bulloides* and *G. inflata* bloom from December to June, i.e., in the cold season, south of 50°N in the North Atlantic. North of 50°N, these species bloom in the warm season (March–November) [*Bé*, 1977; *Deuser and Ross*, 1989]. Field samples may also be affected by bioturbation and other parameters whose influences are difficult to identify. We recognize that the range of potential errors associated with $[B(OH)_4^-/HCO_3^-]_{seawater}$ and hence K_D might be underestimated in the depth domain of 250–350 m for *G. inflata*. Had we assigned shallower habitat depth (e.g., 100 m), the range of calculated K_D for *G. inflata* would be decreased and the sensitivity of K_D on temperature would be weaker. However, the in situ temperature at 100 m is inconsistent with $\delta^{18}O$ temperature [*Elderfield and Ganssen*, 2000]. Further work is needed to improve our K_D estimates and identify possible factors affecting the B incorporation into planktonic foraminiferal calcite. Despite uncertainties in estimated parameters, we believe that relationships obtained using core top samples provide appropriate means for paleoceanographic studies because foraminiferal shells from core tops, which are buried to form the paleoceanographic record, serve as the closest analogue for down core samples.

4.5. Estimation of pH and PCO_2 From Foraminiferal B/Ca

4.5.1. Methodology

[25] The temperature dependence of K_D into planktonic foraminifera provides a method to calculate $[B(OH)_4^-/HCO_3^-]_{seawater}$ from B/Ca by also employing Mg/Ca measured in the same sample to estimate temperature. Mg/Ca temperature is used to compute K_D values using species-specific equations shown in Figure 9a. $[B(OH)_4^-/HCO_3^-]_{seawater}$ values are then obtained by:

$$\left[B(OH)_4^-/HCO_3^-\right]_{seawater} = [B/Ca]_{CaCO_3}/K_D \qquad (4)$$

Pleistocene surface seawater ALK can be approximated from salinity, assuming that both have varied proportionately in the past. With $[B(OH)_4^-/HCO_3^-]_{seawater}$ and ALK in addition to salinity, temperature and pressure (depth), pH and aqueous PCO_2 can then be calculated using CO_2sys.xls (version 12) [*Pelletier et al.*, 2005].

4.5.2. The pH and PCO_2 at ODP Site 668B, Sierra Leone Rise

[26] We calculated $[B(OH)_4^-/HCO_3^-]_{seawater}$ at ODP site 668B from B/Ca and Mg/Ca ratios in *G. ruber* (w) using the K_D-T correlation in Figure 9a and reconstructed pH and PCO_2 by combining ALK estimated from the two salinity models listed in section 4.2 (Figure 10). The errors are estimated according to the method described in *Harris* [2002], using the starting uncertainties of 3% in the calcification temperature (corresponding to 0.76°C on average) [*Hönisch and Hemming*, 2005], 3.5% in B/Ca (corresponding to 3 μmol/mol on average), and 0.08‰ in $\delta^{18}O_{CaCO_3}$. Uncertainties in temperature and $\delta^{18}O_{CaCO_3}$ produce average errors of 0.87 psu and 57 μequ/kg in salinity and alkalinity, respectively. The errors in $[B(OH)_4^-/HCO_3^-]_{seawater}$ shown in Figure 9a are ±10.3% or 0.008 mol/mol on average resulting from uncertainties in the calcification temperature and B/Ca. The final errors associated

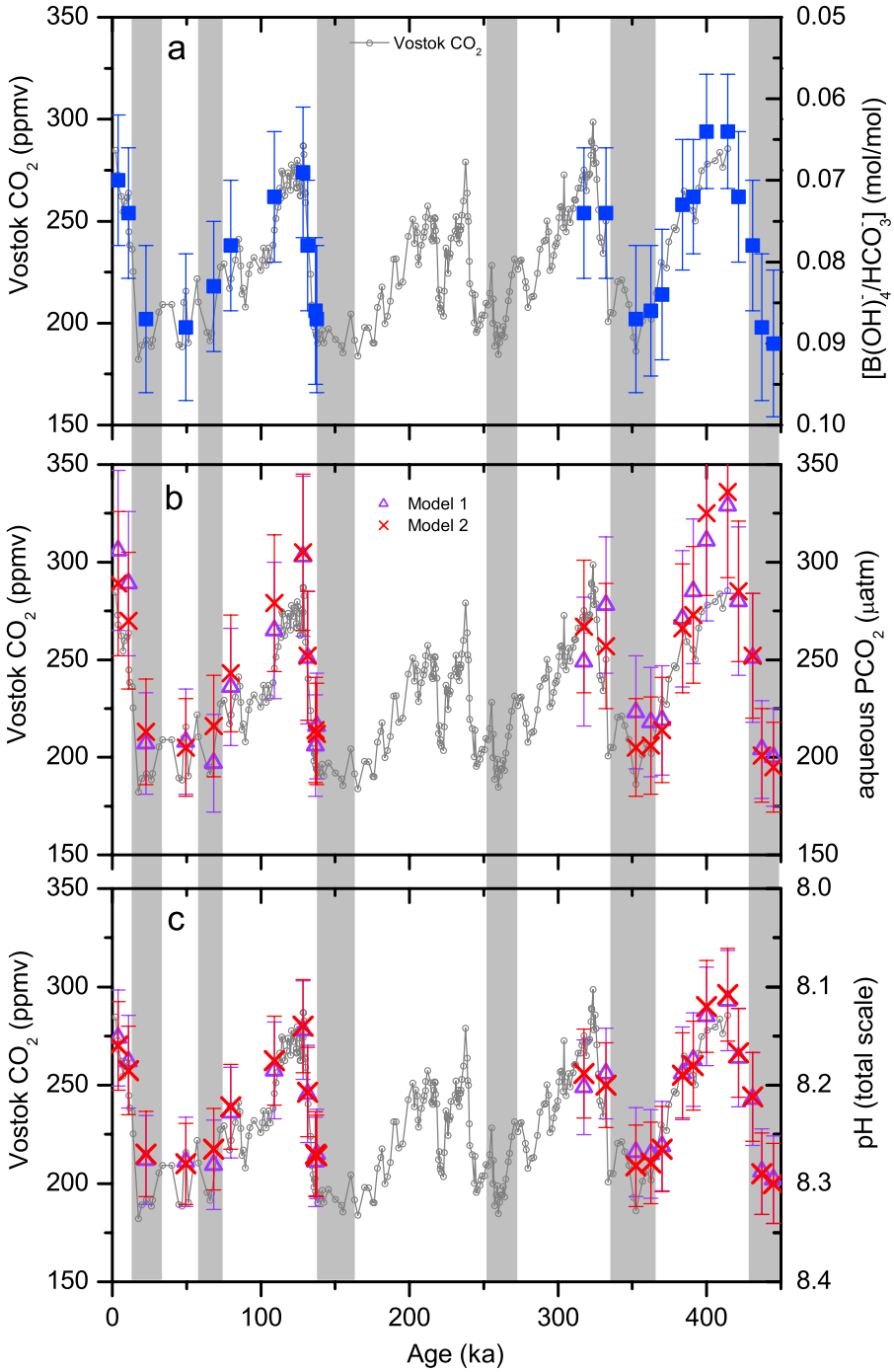

Figure 10. Comparison of atmospheric pCO_2 from the Vostok ice core with seawater $[B(OH)_4^-/HCO_3^-]$ (a), aqueous PCO_2 (b), and pH (c) estimated from foraminiferal B/Ca ratios from ODP 668B. Grey bars indicate glacial intervals.

with pH and PCO_2 are ±0.047 units in pH and ±32 μatm in PCO_2 on average, propagated from the individual uncertainties of $[B(OH)_4^-/HCO_3^-]_{seawater}$ (0.008 mol/mol, corresponding to ±0.042 units in pH and ±30 μatm in PCO_2 on average), temperature (±0.76°C, corresponding to ±0.010 units in pH and ±7 μatm in PCO_2 on average), salinity (±0.87 psu, corresponding to ±0.016 units in pH and ±10 μatm in PCO_2 on average), and ALK (±57 μequ/kg, corresponding to ±0.011 units in pH and ±2 μatm in PCO_2 on average). The reconstructed pH and PCO_2 from B/Ca are consistent with those from $\delta^{11}B$ [*Hönisch and Hemming*, 2005] and resemble the trend of atmospheric

pCO_2 recorded in the Vostok ice core [*Petit et al.*, 1999]. The records from B/Ca and Mg/Ca ratios are at a higher resolution and longer than from $\delta^{11}B$ [*Hönisch and Hemming*, 2005]. However, there is an element of circularity in some calculations because the K_D-T correlation was constructed using $\delta^{11}B$ data from 16 of the 24 samples for which pH was estimated.

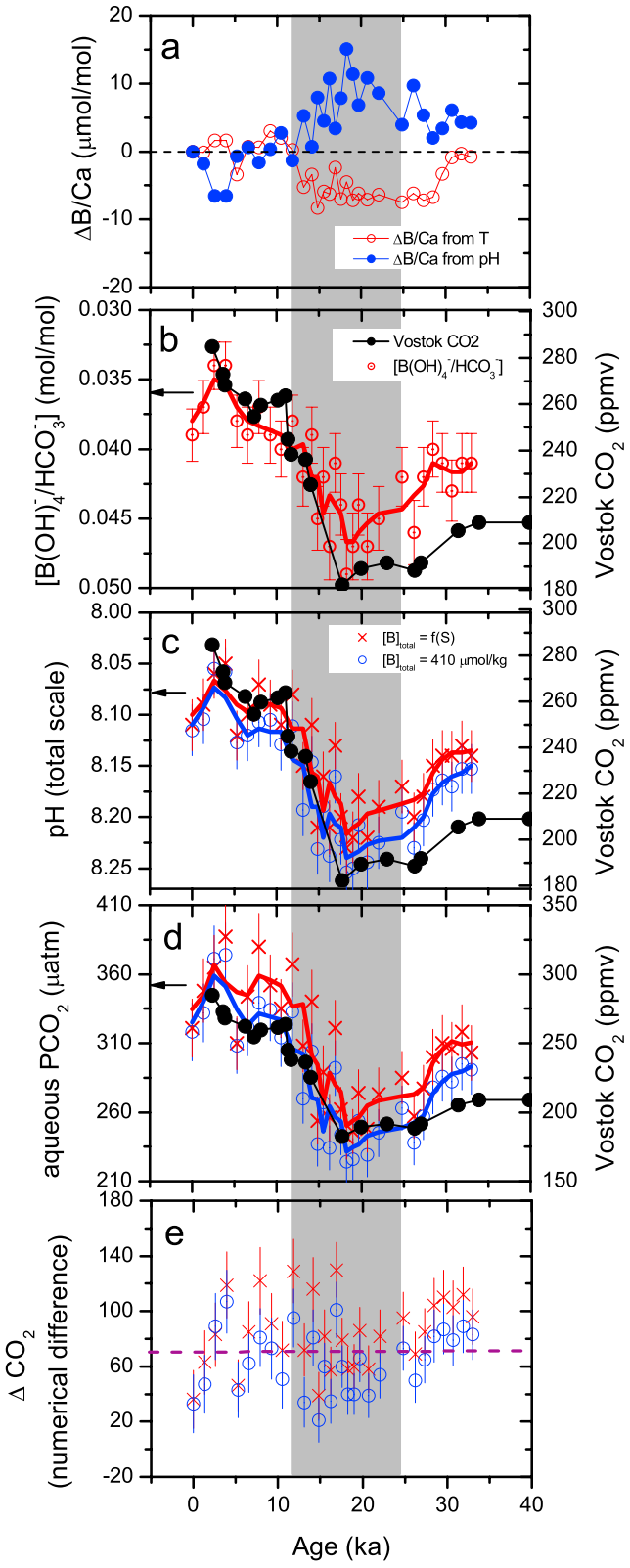

Figure 11. B/Ca changes in *G. inflata* due to changes in temperature and pH (a), calculated seawater $[B(OH)_4^-/HCO_3^-]$ (b), pH (c), partial pressure of aqueous PCO_2 (d), and CO_2 difference between seawater and atmosphere (e) for CHAT 16K. In Figures 11b–11d, solid lines represent 3-point run smoothing of the data. Vostok CO_2 concentrations (solid lines with circles) are also shown for comparison. Arrows indicate preindustrial values at 300 m water depth. In Figure 11d, Vostok pCO_2 and aqueous PCO_2 are plotted on the same scale but offset by 60 ppmv to assist comparisons. The gray bar indicates MIS 2.

4.5.3. The pH and PCO_2 for Core CHAT 16K

[27] Changes in subsurface pH and PCO_2 across termination I were calculated using B/Ca and Mg/Ca ratios measured in *G. inflata* from CHAT 16K in the Southern Ocean (Figure 6) and the K_D-T relationship independently calibrated using core top *G. inflata* from the North Atlantic (Figure 9a). It would be preferable to use shallower dwelling species (e.g., *G. bulloides*), but we selected *G. inflata* because B/Ca measurements are analytically more precise at higher ratio ranges and the K_D-T calibration is well defined. Knowing changes in temperature from Mg/Ca and the sensitivity of K_D on temperature, B/Ca changes due to temperature can be calculated by $\Delta(B/Ca)_T = K_D \times [B(OH)_4^-/HCO_3^-]_{core\ top} - (B/Ca)_{core\ top}$, and the changes in B/Ca caused by pH are: $\Delta(B/Ca)_{pH} = B/Ca - (B/Ca)_{core\ top} - \Delta(B/Ca)_T$. $\Delta(B/Ca)_{pH}$ show higher ratios during glacial than interglacial intervals by ~15 μmol/mol (Figure 11a), consistent with expected variations in seawater $[B(OH)_4^-/HCO_3^-]$ due to variations in atmospheric pCO_2 across termination I (Figure 11b). Compared to $\Delta(B/Ca)_{pH}$, $\Delta(B/Ca)_T$ shows an opposite trend but with a similar amplitude, resulting in small glacial-interglacial variations in overall B/Ca ratios between glacial and interglacial times (Figure 6a).

[28] With $\delta^{18}O_{cc}$ and $SST_{Mg/Ca}$ (section 3.3), the seawater $\delta^{18}O_{sw}$ is calculated using equation: $\delta^{18}O_{sw} = (\delta^{18}O_{cc} + 0.27) - [4.38 - (4.38^2 - 4 \times 0.1 \times (16.9 - SST))^{0.5}]/(2 \times 0.1)$ [*O'Neil et al.*, 1969]. As a first approximation, salinity and ALK are estimated assuming that the local S-$\delta^{18}O_{sw}$ and ALK-S relationships have remained constant in the past. $\delta^{18}O_{sw}$ is converted into a local salinity record by using a S-$\delta^{18}O_{sw}$ relation on the basis of surface ocean data from latitudes 30–50°S, longitudes 160–180°W, and water depth <500 m compiled by *Schmidt et al.* [1999]: $S = 34.28 + 1.983 \times \delta^{18}O_{sw}$ ($R^2 = 0.88$). Compilation of the GLODAP data set for the same water mass indicates that modern ALK and S can be described by a linear fit of the form $ALK = 43.173 \times S + 798.62$ ($R^2 = 0.89$) [*Key et al.*, 2004]. The S-$\delta^{18}O_{sw}$ and ALK-S relationships for narrower depth intervals (e.g., 250–350 m) are similar to those based on data from 0–500 m water depth. Measurements of $\delta^{18}O$ in *G. inflata* collected from the sediment trap deployed (42°S) at North Chatham Rise (NCR) show a range of 0.4–1.4‰, placing this species at the average habitat depth of ~50 m [*King and Howard*, 2005]. By comparison, $\delta^{18}O$ in Holocene *G. inflata* from CHAT 16K show much higher values

(1.79 ± 0.43‰ for 0–5 ka) (Figure 6c), matching calculated $\delta^{18}O_{cc}$ at 300 m depth (see Figure 6a by *King and Howard* [2005]). The core top $[B(OH)_4^-/HCO_3^-]_{seawater}$ calculated from B/Ca and Mg/Ca is also roughly similar to the modern value at 300 m (Figure 11b). Therefore we used 300 m water depth for our calculations. The deeper apparent calcification depth of *G. inflata* from CHAT 16K might be due to selection of larger (300–355μm) shells used in our study [*Lončarić et al.*, 2006].

[29] Using the CO_2sys.xls (version 12) [*Pelletier et al.*, 2005] and dissociation constants employed in section 2.2, we can translate reconstructed seawater $[B(OH)_4^-/HCO_3^-]$ and estimated alkalinity values into pH and PCO_2 estimates (Table 3 and Figures 11c and 11d). Two scenarios are considered to estimate $[B]_{tot}$: (1) $[B]_{tot}$ changed proportionately with S [*Uppstrom*, 1974] and (2) $[B]_{tot}$ remained constant at 410 μmol/kg (the modern value) in the past. Using the procedure given in section 4.5.2, the average errors in $[B(OH)_4^-/HCO_3^-]_{seawater}$ are ±0.002 mol/mol caused by uncertainties of ±0.8°C in temperature [*Mashiotta et al.*, 1999] and ~±2 μmol/mol (±3.5%) in B/Ca. The average errors in pH and PCO_2 are ±0.024 units and ±20 μatm, respectively, propagated from uncertainties in $[B(OH)_4^-/HCO_3^-]_{seawater}$ (±0.002 mol/mol, corresponding to ±0.020 units in pH and ±16 μatm in PCO_2 on average), temperature (±0.8°C, corresponding to ±0.010 units in pH and ±9 μatm in PCO_2 on average), S (±0.40 psu, corresponding to ±0.008 units in pH and ±6 μatm in PCO_2 on average), and ALK (±17 μequ/kg, corresponding to ±0.002 units in pH and ±1 μatm in PCO_2 on average). Considering these errors, the reconstructed pH and PCO_2 using different $[B]_{tot}$ scenarios show good agreement, indicating that variations in $[B(OH)_4^-/HCO_3^-]$ mainly reflect past changes in seawater pH.

[30] The reconstructed seawater pH and PCO_2 parallel the evolution trend of atmospheric pCO_2 recorded in the Vostok ice core [*Petit et al.*, 1999]. The calculated pH values reveal that the LGM surface ocean pH is ~+0.15 units higher than the Holocene at the habitat depth of *G. inflata* (~300 m) at site CHAT 16K (Figure 11c), similar to the previously determined glacial–interglacial pH difference of 0.2 ± 0.1 in tropical Atlantic and Pacific using $\delta^{11}B$ [*Sanyal et al.*, 1997; *Sanyal and Bijma*, 1999; *Hönisch and Hemming*, 2005]. The estimated LGM PCO_2 (~255 μatm) is lower than for the Holocene (~350 μatm) by ~95 μatm, matching glacial-interglacial atmospheric pCO_2 differences recorded in the ice core [*Petit et al.*, 1999] (Figure 11d). Foraminiferal shell weight measurements on *G. inflata* indicate higher surface seawater $[CO_3^{2-}]$ during the last glacial time at CHAT 16K [*Barker and Elderfield*, 2002; *Greaves*, 2007]. The calculated aqueous PCO_2 values are consistently ~70 ppm higher than atmospheric pCO_2 (Figure 11e), perhaps caused by decomposition of particulate organic matter at the habitat depth of *G. inflata*. Planktonic Cd/Ca results imply that the nutrient concentration of the surface ocean in the glacial Southern Ocean was not significantly different from today [*Elderfield and Rickaby*, 2000], suggesting a similar biochemical influence on PCO_2 and possibly a similar vertical PCO_2 gradient in surface water. Therefore the constant CO_2 difference recorded by *G. inflata* might indicate that the net sea-air CO_2 flux has not been significantly changed at site CHAT 16K since the last glacial.

5. Conclusions

[31] On the basis of B/Ca measurements in planktonic foraminifera from the North Atlantic Ocean, the Southern Ocean, and ODP site 668B in the eastern equatorial Atlantic, B/Ca ratios are not affected by dissolution on the seafloor but are strongly influenced by ambient seawater pH and temperature. Calcification temperatures from Mg/Ca can be used to determine K_D and to extract seawater pH changes from residual B/Ca variations. The calculated PCO_2 using B/Ca and Mg/Ca ratios in *G. inflata* from CHAT 16K mimic atmospheric pCO_2 recorded in the Vostok ice core, demonstrating the feasibility of using B/Ca in planktonic foraminifera for PCO_2 reconstructions. The pH and PCO_2 reconstructions at ODP 668B and CHAT 16K indicate that the ocean-atmosphere CO_2 flux has not been substantially changed in these locations. Further studies are needed to better calibrate the temperature and pH effects on K_D and B/Ca in planktonic foraminifera.

[32] **Acknowledgments.** We are grateful to Mervyn Greaves for permission to use his unpublished Mg/Ca data for CHAT 16K. We are very grateful to Gerald Ganssen for access to foraminifera from the APNAP project. Samples from the NEAPACC project were collected with NERC funding to Nick McCave, Nick Shackleton, and H.E. We also thank the Ocean Drilling Program (ODP) for core samples, Jason Day and Mervyn Greaves for laboratory assistance, Matthew Schmidt for helping with salinity reconstructions, Martin Palmer, Alex Piotrowski, and Johannes Simstich for discussion, and Linda Booth for help with foraminifera picking. We are grateful for the constructive comments from Editor Eelco Rohling and the reviews of Howie Spero and an anonymous reviewer which have improved this paper. This research was funded by the Gates Cambridge Trust, European Union 5th Framework Programme project 6C (EVK2-CT-2002-00135), NERC and the Gary Comer Foundation.

References

Al-Ammar, A., R. K. Gupta, and R. M. Barnes (1999), Elimination of boron memory effect in inductively coupled plasma-mass spectrometry by addition of ammonia, *Spectrochim. Acta, Part B*, *54*, 1077–1084.

Al-Ammar, A., E. Reitznerova, and R. M. Barnes (2000), Improving boron isotope ratio measurement precision with quadrupole inductively coupled plasma-mass spectrometry, *Spectrochim. Acta, Part B*, *55*, 1861–1867.

Anand, P., H. Elderfield, and M. H. Conte (2003), Calibration of Mg/Ca thermometry in planktonic foraminifera from a sediment trap time series, *Paleoceanography*, *18*(2), 1050, doi:10.1029/2002PA000846.

Barker, S. (2002), Planktonic foraminiferal proxies for temperature and pCO_2, Ph.D. thesis, 136 pp., Univ. of Cambridge, U. K.

Barker, S., and H. Elderfield (2002), Foraminiferal calcification response to glacial-interglacial changes in atmospheric CO_2, *Science*, *297*, 833–836.

Barker, S., M. Greaves, and H. Elderfield (2003), A study of cleaning procedures used for foraminiferal Mg/Ca paleothermometry, *Geochem. Geophys. Geosyst.*, *4*(9), 8407, doi:10.1029/2003GC000559.

Bé, A. W. H. (1977), An ecological, zoogeographic and taxonomic review of recent planktonic foraminifera, in *Oceanic Micropaleontology*, edited

by A. T. S. Ramsey, pp. 1–100, Elsevier, New York.

Bird, M. I., and J. A. Cali (2002), A revised high-resolution oxygen-isotope chronology for ODP-668B: Implications for Quaternary biomass burning in Africa, *Global Planet. Change*, *33*, 73–76.

Boyle, E. A., and L. D. Keigwin (1985–1986), Comparison of Atlantic and Pacific paleochemical records for the last 215,000 years: Changes in deep ocean circulation and chemical inventories, *Earth Planet. Sci. Lett.*, *76*, 135–150.

Brown, S. J., and H. Elderfield (1996), Variations in Mg/Ca and Sr/Ca ratios of planktonic foraminifera caused by postdepositional dissolution: Evidence of shallow Mg-dependent dissolution, *Paleoceanography*, *11*, 543–551.

Deuser, W. G., and E. H. Ross (1989), Seasonally abundant planktonic foraminifera of the Sargasso Sea: Succession, deep-water fluxes, isotopic compositions, and paleoceanographic implications, *J. Foraminiferal Res.*, *19*, 268–293.

Dickson, A. G. (1990), Thermodynamics of the dissociation of boric-acid in synthetic seawater from 273.15-k to 318.15-k, *Deep Sea Res., Part A*, *37*, 755–766.

Dickson, A. G., and F. J. Millero (1987), A comparison of the equilibrium constants for the dissociation of carbonic acid in seawater media, *Deep Sea Res., Part A*, *34*, 1733–1743.

Elderfield, H., and G. Ganssen (2000), Past temperature and $\delta^{18}O$ of surface ocean waters inferred from foraminiferal Mg/Ca ratios, *Nature*, *405*, 442–445.

Elderfield, H., and R. E. M. Rickaby (2000), Oceanic Cd/P ratio and nutrient utilization in the glacial Southern Ocean, *Nature*, *405*, 305–310.

Elderfield, H., C. J. Bertram, and J. Erez (1996), A biomineralization model for the incorporation of trace elements into foraminiferal calcium carbonate, *Earth Planet. Sci. Lett.*, *142*, 409–423.

Elderfield, H., M. Cooper, and G. Ganssen (2000), Sr/Ca in multiple species of planktonic foraminifera: Implications for reconstructions of seawater Sr/Ca, *Geochem. Geophys. Geosyst.*, *1*, doi:10.1029/1999GC000031.

Elderfield, H., M. Vautravers, and M. Cooper (2002), The relationship between shell size and Mg/Ca, Sr/Ca, $\delta^{18}O$, and $\delta^{13}C$ of species of planktonic foraminifera, *Geochem. Geophys. Geosyst.*, *3*(8), 1052, doi:10.1029/2001GC000194.

Erez, J., and S. Honjo (1981), Comparison of isotopic composition of planktonic-foraminifera in plankton tows, sediment traps and sediments, *Palaeogeogr. Palaeoclimatol. Palaeoecol.*, *33*, 129–156.

Fairbanks, R. G., M. Sverdlove, R. Free, P. H. Wiebe, and A. W. H. Be (1982), Vertical-distribution and isotopic fractionation of living planktonic-foraminifera from the Panama Basin, *Nature*, *298*, 841–844.

Fallon, S. J., M. T. McCulloch, R. Woesik, and D. J. Sinclair (1999), Coral at their latitudinal limits: Laser ablation trace element systematics in Porites from Shirigai Bay, Japan, *Earth Planet. Sci. Lett.*, *172*, 221–238.

Ganssen, G. M., and D. Kroon (2000), The isotopic signature of planktonic foraminifera from NE Atlantic surface sediments: Implications for the reconstruction of past oceanic conditions, *J. Geol. Soc.*, *157*, 693–699.

Greaves, M. (2007), Trace elements in marine biogenic carbonates: Analyses and applications in studies of past ocean chemistry, Ph.D. thesis, Univ. of Southampton, U. K.

Harris, D. C. (2002), *Quantitative Chemical Analysis*, 744 pp., W. H. Freeman, New York.

Hemming, N. G., and G. N. Hanson (1992), Boron isotopic composition and concentration in modern marine carbonates, *Geochim. Cosmochim. Acta*, *56*, 537–543.

Hemming, N. G., R. J. Reeder, and S. R. Hart (1998), Growth-step-selective incorporation of boron on the calcite surface, *Geochim. Cosmochim. Acta*, *62*, 2915–2922.

Hobbs, M. Y., and E. J. Reardon (1999), Effect of pH on boron coprecipitation by calcite: Further evidence for nonequilibrium partitioning of trace elements, *Geochim. Cosmochim. Acta*, *63*, 1013–1021.

Hönisch, B., and N. G. Hemming (2004), Ground-truthing the boron isotope-paleo-pH proxy in planktonic foraminifera shells: Partial dissolution and shell size effects, *Paleoceanography*, *19*, PA4010, doi:10.1029/2004PA001026.

Honisch, B., and N. G. Hemming (2005), Surface ocean pH response to variations in pCO_2 through two full glacial cycles, *Earth Planet. Sci. Lett.*, *236*, 305–314.

Hönisch, B., J. Bijma, A. D. Russell, H. J. Spero, M. R. Palmer, R. E. Zeebe, and A. Eisenhauer (2003), The influence of symbiont photosynthesis on the boron isotopic composition of foraminifera shells, *Mar. Micropaleontol.*, *49*, 87–96.

Key, R. M., et al. (2004), A global ocean carbon climatology: Results from Global Data Analysis Project (GLODAP), *Global Biogeochem. Cycles*, *18*(4), GB4031, doi:10.1029/2004GB002247.

King, A. L., and W. R. Howard (2005), $\delta^{18}O$ seasonality of planktonic foraminifera from Southern Ocean sediment traps: Latitudinal gradients and implications for paleoclimate reconstructions, *Mar. Micropaleontol.*, *56*, 1–24.

Lemarchand, D., J. Gaillardet, E. Lewin, and C. J. Allegre (2000), The influence of rivers on marine boron isotopes and implications for reconstructing past ocean pH, *Nature*, *408*, 951–954.

Lemarchand, D., J. Gaillardet, E. Lewin, and C. J. Allegre (2002), Boron isotope systematics in large rivers: Implications for the marine boron budget and paleo-pH reconstruction over the Cenozoic, *Chem. Geol.*, *190*, 123–140.

Lewis, E., and D. W. R. Wallace (1998), Program developed for CO_2 system calculations, *Rep. ORNL/CDIAC-105*, Carbon Dioxide Inf. Anal. Cent. Oak Ridge Natl. Lab. U. S. Dept. of Energy, Oak Ridge, Tenn.

Lončarić, N., F. J. C. Peeters, D. Kroon, and G.-J. A. Brummer (2006), Oxygen isotope ecology of recent planktic foraminifera at the central Walvis Ridge (SE Atlantic), *Paleoceanography*, *21*, PA3009, doi:10.1029/2005PA001207.

Marchitto, T. M., W. B. Curry, and D. W. Oppo (2000), Zinc concentrations in benthic foraminifera reflect seawater chemistry, *Paleoceanography*, *15*, 299–306.

Mashiotta, T. A., D. W. Lea, and H. J. Spero (1999), Glacial-interglacial changes in Subantarctic sea surface temperature and $\delta^{18}O_{water}$ using foraminiferal Mg, *Earth Planet. Sci. Lett.*, *170*, 417–432.

Mehrbach, C., C. H. Culberso, J. E. Hawley, and R. M. Pytkowic (1973), Measurement of apparent dissociation-constants of carbonic-acid in seawater at atmospheric-pressure, *Limnol. Oceanogr.*, *18*, 897–907.

Mortyn, P. G., and C. D. Charles (2003), Planktonic foraminiferal depth habitat and $\delta^{18}O$ calibrations: Plankton tow results from the Atlantic sector of the Southern Ocean, *Paleoceanography*, *18*(2), 1037, doi:10.1029/2001PA000637.

O'Neil, J. R., R. N. Slayton, and T. K. Mayeda (1969), Oxygen isotope fractionation in divalent metal carbonates, *J. Chem. Phys.*, *51*, 5547–5558.

Palmer, M. R., and P. N. Pearson (2003), A 23,000-year record of surface water pH and PCO_2 in the western equatorial Pacific Ocean, *Science*, *300*, 480–482.

Palmer, M. R., P. N. Pearson, and S. J. Cobb (1998), Reconstructing past ocean pH-depth profiles, *Science*, *282*, 1468–1471.

Pearson, P. N., and M. R. Palmer (1999), Middle Eocene seawater pH and atmospheric carbon dioxide concentrations, *Science*, *284*, 1824–1826.

Pearson, P. N., and M. R. Palmer (2000), Atmospheric carbon dioxide concentrations over the past 60 million years, *Nature*, *406*, 695–699.

Pelletier, G., E. Lewis, and D. Wallace (2005), A calculator for the CO_2 system in seawater for Microsoft Excel/VBA, report, Wash. State Dept. of Ecol., Olympia.

Petit, J. R., et al. (1999), Climate and atmospheric history of the past 420,000 years from the Vostok ice core, Antarctica, *Nature*, *399*, 429–436.

Rickaby, R. E. M., and H. Elderfield (1999), Planktonic foraminiferal Cd/Ca: Paleonutrients or paleotemperature?, *Paleoceanography*, *14*, 293–303.

Rosenthal, Y., and E. A. Boyle (1993), Factors controlling the fluoridecontent of planktonic foraminifera: An evaluation of its paleoceanographic applicability, *Geochim. Cosmochim. Acta*, *57*, 335–346.

Rosenthal, Y., E. A. Boyle, and N. Slowey (1997), Temperature control on the incorporation of magnesium, strontium, fluorine, and cadmium into benthic foraminiferal shells from Little Bahama Bank: Prospects for thermocline paleoceanography, *Geochim. Cosmochim. Acta*, *61*, 3633–3643.

Russell, A. D., B. Honisch, H. J. Spero, and D. W. Lea (2004), Effects of seawater carbonate ion concentration and temperature on shell U, Mg, and Sr in cultured planktonic foraminifera, *Geochim. Cosmochim. Acta*, *68*, 4347–4361.

Sanyal, A., and J. Bijma (1999), A comparative study of the northwest Africa and eastern equatorial Pacific upwelling zones as sources of CO_2 during glacial periods based on boron isotope paleo-pH estimation, *Paleoceanography*, *14*, 753–759.

Sanyal, A., N. G. Hemming, G. N. Hanson, and W. S. Broecker (1995), Evidence for a higher pH in the glacial ocean from boron isotopes in foraminifera, *Nature*, *373*, 234–236.

Sanyal, A., N. G. Hemming, W. S. Broecker, D. W. Lea, H. J. Spero, and G. N. Hanson (1996), Oceanic pH control on the boron isotopic composition of foraminifera: Evidence from culture experiments, *Paleoceanography*, *11*, 513–517.

Sanyal, A., N. G. Hemming, W. S. Broecker, and G. N. Hanson (1997), Changes in pH in the eastern equatorial Pacific across stage 5–6 boundary based on boron isotopes in foraminifera, *Global Biogeochem. Cycles*, *11*, 125–133.

Sanyal, A., M. Nugent, R. J. Reeder, and J. Buma (2000), Seawater pH control on the

boron isotopic composition of calcite: Evidence from inorganic calcite precipitation experiments, *Geochim. Cosmochim. Acta*, *64*, 1551–1555.

Sanyal, A., J. Bijma, H. Spero, and D. W. Lea (2001), Empirical relationship between pH and the boron isotopic composition of *Globigerinoides sacculifer*: Implications for the boron isotope paleo-pH proxy, *Paleoceanography*, *16*, 515–519.

Schmidt, G. A., G. R. Bigg, and E. J. Rohling (1999), Global Seawater Oxygen-18 Database, http://data.giss.nasa.gov/o18data, Goddard Inst. for Space Stud., New York.

Sikes, E. L., W. R. Howard, H. L. Neil, and J. K. Volkman (2002), Glacial-interglacial sea surface temperature changes across the subtropical front east of New Zealand based on alkenone unsaturation ratios and foraminiferal assemblages, *Paleoceanography*, *17*(2), 1012, doi:10.1029/2001PA000640.

Sinclair, D. (2005), Correlated trace element "vital effects" in tropical corals: A new geochemical tool for probing biomineralization, *Geochim. Cosmochim. Acta*, *69*, 3265–3284.

Sinclair, D., L. Kinsley, and M. McCulloch (1998), High resolution analysis of trace elements in corals by laser ablation ICP-MS, *Geochim. Cosmochim. Acta*, *212*, 1889–1901.

Spero, H. J., J. Bijma, D. W. Lea, and B. E. Bemis (1997), Effect of seawater carbonate concentration on foraminiferal carbon and oxygen isotopes, *Nature*, *390*, 497–500.

Spero, H. J., K. M. Mielke, E. M. Kalve, D. W. Lea, and D. K. Pak (2003), Multispecies approach to reconstructing eastern equatorial Pacific thermocline hydrography during the past 360 kyr, *Paleoceanography*, *18*(1), 1022, doi:10.1029/2002PA000814.

Spivack, A. J., and J. M. Edmond (1987), Boron isotope exchange between seawater and the oceanic-crust, *Geochim. Cosmochim. Acta*, *51*, 1033–1043.

Spivack, A. J., C. F. You, and H. J. Smith (1993), Foraminiferal boron isotope ratios as a proxy for surface ocean pH over the past 21-Myr, *Nature*, *363*, 149–151.

Uppstrom, L. R. (1974), Boron/chlorinity ratio of deep-sea water from pacific ocean, *Deep Sea Res. Oceanogr. Abstr.*, *21*, 161–162.

U.S. Department of Energy (1994), *Handbook of Methods for the Analysis of the Various Parameters of the Carbon Dioxide System in Seawater*, Washington, D. C.

Wara, M. W., M. L. Delaney, T. D. Bullen, and A. C. Ravelo (2003), Possible roles of pH, temperature, and partial dissolution in determining boron concentration and isotopic composition in planktonic foraminifera, *Paleoceanography*, *18*(4), 1100, doi:10.1029/2002PA000797.

Weaver, P. P. E., H. Neil, and L. Carter (1997), Sea surface temperature estimates from the southwest Pacific based on planktonic foraminifera and oxygen isotopes, *Palaeogeogr. Palaeoclimatol. Palaeoecol.*, *131*, 241–256.

Weaver, P. P. E., L. Carter, and H. L. Neil (1998), Response of surface water masses and circulation to late Quaternary climate change east of New Zealand, *Paleoceanography*, *13*, 70–83.

Wilke, I., T. Bickert, and F. J. C. Peeters (2006), The influence of seawater carbonate ion concentration [CO_3^{2-}] on the stable carbon isotope composition of the planktic foraminifera species Globorotalia inflata, *Mar. Micropaleontol.*, *58*, 243–258.

Wolf-Gladrow, D. A., J. Bijma, and R. E. Zeebe (1999), Model simulation of the carbonate chemistry in the microenvironment of symbiont bearing foraminifera, *Mar. Chem.*, *64*, 181–198.

Yu, J. M. (2006), Boron concentration in foraminifera as a proxy for glacial-interglacial change in the oceanic carbonate system, Ph.D. thesis, 155 pp., Univ. of Cambridge, U. K.

Yu, J. M., J. Day, M. Greaves, and H. Elderfield (2005), Determination of multiple element/calcium ratios in foraminiferal calcite by quadrupole ICP-MS, *Geochem. Geophys. Geosyst.*, *6*, Q08P01, doi:10.1029/2005GC000964.

Zeebe, R. E., and D. A. Wolf-Gladrow (2001), *CO_2 in Seawater: Equilibrium, Kinetics, Isotopes*, *Elsevier Oceanogr. Ser.*, vol. 65, Elsevier, New York.

Zeebe, R. E., D. A. Wolf-Gladrow, J. Bijma, and B. Hönisch (2003), Vital effects in foraminifera do not compromise the use of $\delta^{11}B$ as a paleo-pH indicator: Evidence from modeling, *Paleoceanography*, *18*(2), 1043, doi:10.1029/2003PA000881.

H. Elderfield and J. Yu, Godwin Laboratory for Palaeoclimate Research, Department of Earth Sciences, University of Cambridge, Downing Street, Cambridge, CB2 3EQ, UK. (jyu02@esc.cam.ac.uk)

B. Hönisch, Lamont-Doherty Earth Observatory of Columbia University, Palisades, NY 10964-8000, USA.